Research Paper
Computational Methods for Differential Equations
http://cmde.tabrizu.ac.ir
Vol. *, No. *, *, pp. 1-22
DOI:10.22034/cmde.2025.63426.2831

Robust numerical approach for singularly perturbed parabolic problems with discontinuous convection coefficients and source terms

Shegaye Lema Cheru[1,*], **Gemechis File Duressa**[2], **and Tariku Birabasa Mekonnen**[1]
[1]Department of Mathematics, Wollega University, Nekemte, Ethiopia.
[2]Department of Mathematics, Jimma University, Jimma, Ethiopia.

Abstract

This study explores the numerical method of $1-D$ singularly perturbed parabolic problems, influenced by two distinct parameters affecting diffusion and convection. With discontinuous convection and source terms, the solutions exhibit boundary and interior layers due to the perturbations and discontinuities. The time variable is first discretized using the implicit Euler method on a uniform mesh, followed by spatial discretization of the semi-discrete problems with a non-polynomial cubic spline incorporating an exponential fitting factor. The method is shown to be first-order accurate and uniformly convergent. Its efficiency is demonstrated through four test cases, yielding more precise results than those reported in existing methods.

Keywords. Singularly perturbed problems, Discontinuous convection and source term, Implicit Euler Method, Non-polynomial cubic spline.
2010 Mathematics Subject Classification. 65L11,65M06,65M12,65M22.

1. Introduction

In many real mathematical models, the goal is to focus on key variables while ignoring those with minor effects from small parameters. A model influenced by small parameter is termed regularly or singularly perturbed. In singularly perturbed problems(SPPs), small parameters affect higher-order derivatives, reducing the order of differential equations when set to zero. The reduced solution fails to meet boundary conditions, reflecting the multi-scale nature of the solution. These regions, where the solutions changes rapidly, are called layer regions. The existence and position of boundary layers in reaction-convection-diffusion problems are dictated by the quantity of parameters present [2, 3, 21]. These layers develop at boundaries where substantial variations take place. Additionally, interior layers arise when the coefficients, source term, or boundary conditions lack sufficient smoothness [6, 7, 10, 12].

Here, we consider parabolic reaction-convection-diffusion problems, incorporating two perturbation parameters that have a discontinuous coefficients and source terms.

$$\begin{cases} \Phi_{\varepsilon,\mu}u(x,t) \equiv \varepsilon\dfrac{\partial^2 u}{\partial x^2}(x,t) + \mu a(x,t)\dfrac{\partial u}{\partial x}(x,t) - b(x,t)u(x,t) - \\ c(x,t)\dfrac{\partial u}{\partial t}(x,t) = \varpi(x,t), (x,t) \in \mathfrak{Q}^- \cup \mathfrak{Q}^+, \\ u(0,t) = \vartheta(t) \quad \text{in} \quad \mathfrak{Q}_l, \quad u(1,t) = \xi(t) \quad \text{in} \quad \mathfrak{Q}_r, \\ u(x,0) = \phi(x) \quad \text{in} \quad \mathfrak{Q}_b, \\ |[a](\varphi)| \le C, \quad |[\varpi](\varphi)| \le C, \\ a(x,t) \le -\alpha_1 < 0, \quad (x,t) \in \mathfrak{Q}^-, \\ a(x,t) \ge \alpha_2 > 0, \quad (x,t) \in \mathfrak{Q}^+, \\ b(x,t) \ge \beta > 0, \quad c(x,t) \ge c > 0. \end{cases} \tag{1.1}$$

Received: 09 September 2024 ; Accepted: 24 August 2025.
∗ Corresponding author. Email: shegaye04@gmail.com, shegayel@wollegauniversity.edu.et.

Here, $0<\varepsilon \ll 1, 0 \leq \mu \leq 1$ are perturbation parameters. The domains are specified in Figure 1 as follows: $\mathfrak{Q} = \Omega \times (0,T], \mathfrak{Q}^- = \Omega^- \times (0,T], \mathfrak{Q}^+ = \Omega^+ \times (0,T], \mathfrak{M} = \overline{\mathfrak{Q}} \setminus \mathfrak{Q}$, where $\Omega = (0,1), \Omega^- = (0,\varphi), \Omega^+ = (\varphi,1)$ and the boundaries are defined as $\mathfrak{Q}_l = \{(0,t) : 0 \leq t \leq T\}, \mathfrak{Q}_r = \{(1,t) : 0 \leq t \leq T\}, \mathfrak{Q}_b = \mathfrak{Q}_b^- \cup \mathfrak{Q}_b^+$, where, $\mathfrak{Q}_b^- = [0,\varphi] \times \{t=0\}$ and $\mathfrak{Q}_b^+ = [\varphi,1] \times \{t=0\}$. We also denote $\mathfrak{M} = \mathfrak{Q}_b \cup \mathfrak{Q}_l \cup \mathfrak{Q}_r$ and $\mathfrak{M}^{\pm} = \{(\varphi,t) : 0 \leq t \leq T\}$. The terms $a(x,t), \varpi(x,t)$

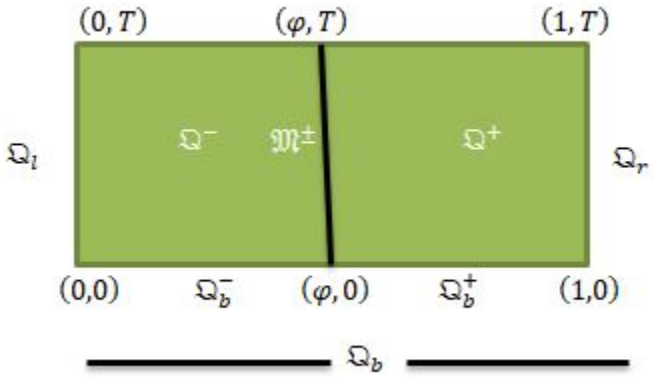

FIGURE 1. Domain $\mathfrak{Q} = [0,1] \times (0,T]$.

are smooth enough in $(\mathfrak{Q}^- \cup \mathfrak{Q}^+) \cup \mathfrak{Q}$ and $b(x,t), c(x,t)$ are continuous in $\mathfrak{Q}$. Both terms $a(x,t)$ and $\varpi(x,t)$ has a discontinuity at $\varphi \in \Omega$, symbolized by $[\psi](\varphi,t) = [\psi](\varphi+,t) - [\psi](\varphi-,t)$. If $a(x,t)$ changes sign across the discontinuity, a solution exist for convection-diffusion problems with discontinuous first derivative coefficient. The discontinuities in convection and source terms generate interior layers on either side of the discontinuity at $x = \varphi$. The small diffusion parameter causes two boundary layers in the outcome of Eq. (1.1) and the sign of $a(x,t)$ and the ratio between diffusion and the square of convection parameter determine the behavior of layers. Specifically, interior layer form on either side of the discontinuity, and boundary layer widths are continuously influenced by these ratios.

Numerous numerical techniques have been developed for two-parameter singularly perturbed problems(TP-SPPs) with smooth data [1, 5, 7, 8, 11, 14–18, 20, 22, 23]; however, in the case of non-smooth data, the numerical study is restricted, and the methods for TP-SPPs with discontinuous data are still in the early stages of development. Daba and Duressa [9] considers a computational technique for a class of SPPs with discountinuous coefficients involving negative shifts. First-order convergent scheme with a discontinuity in the source term was developed by Clavero et al. [6] for TP-SPPs. In the case of Eq. (1.1), Chandru et al. [2] propose the scheme that consists of an upwind schemes in spatial and backward Euler in temporal. Chandru [3] created parameter uniform numerical scheme for Eq. (1.1) on adaptive mesh. Kumar and Kumari [13] developed a nearly first-order uniformly convergent schemes, combining the Crank-Nicolson scheme on a uniform temporal grid with an upwind difference scheme applied to a specified Shishkin mesh. For a class of TP-SPPs with discountinuous convection and source terms, Singh et al. [21] developed a spline-based numerical technique. The authors discretized the problem using Crank-Nicolson scheme for the time dimension and the trigonometric B-spline basis for the spatial dimensions.

In this work, we examine a TP-SPPs reaction-convection-diffusion problems in $1-D$ with discontinuous convection coefficient and source terms. Only a few researchers, specifically [2, 3, 13, 21], have investigated the problem at hand. In the context of TP-SPPSs with discontinuous convection coefficients and source terms, a prominent gap exists in the literature regarding the application of spline methods. Although spline methods have shown success in treating TP-SPPs with smooth data (see [8, 15]), more research is needed to address discontinuous data types. In the context of spline-based methods, this gap offers a chance to create an accurate numerical treatment to address the difficulties caused by two perturbation parameters and discountinous source terms. Inspired by the previously mentioned research, we will examine TP-SPPs that contain non-smooth data in the source term and convection coefficient.

This study emphasizes a parameter-uniform numerical approach for TP-SPPs, where discontinuities in the source term and convection coefficient within the domain lead to the formation of an interior layer, separate from the boundary layers. The proposed method combines a non-polynomial cubic spline technique for spatial discretization with the implicit Euler method for temporal discretization. To the best of our knowledge, there is limited research on exponentially fitted methods for singularly perturbed parabolic problems with discontinuous convection coefficients and source terms. While many studies focus on smooth or piecewise continuous cases, the challenges posed by strong singular perturbations and discontinuities remain largely unexplored. Unlike prior work using piecewise uniform Shishkin meshes, our novel approach employs a uniform mesh, achieving greater accuracy.

2. Analytical Properties of Continuous problem

Here, we investigate the relevance of the bounds on derivatives, which are based on Eq. (1.1).

Lemma 2.1. *Eq.* (1.1) *has a solution* $u(x,t) \in C^0\left(\overline{\mathfrak{Q}}\right) \cap C^1\left(\mathfrak{Q}\right) \cap C^2\left(\mathfrak{Q}^- \cup \mathfrak{Q}^+\right)$.

Proof. The proof is by constructin(see [10]). Consider the function $u_1(x,t)$ and $u_2(x,t)$, which meet, respectively, the subsequent SPDEs:

$$\begin{aligned}
&\left(\varepsilon u_{1xx} + \mu a_1 u_{1x} - b u_1 - c u_{1t}\right)(x,t) = \varpi(x,t), (x,t) \in \mathfrak{Q}^-, \quad \text{and} \\
&\left(\varepsilon u_{2xx} + \mu a_2 u_{2x} - b u_2 - c u_{2t}\right)(x,t) = \varpi(x,t), (x,t) \in \mathfrak{Q}^+,
\end{aligned}$$

where $a_1(x,t), a_2(x,t) \in C^2\left(\mathfrak{Q}\right)$ are structured in a way that these extended functions fulfill:

$$\begin{aligned}
&a_1(x,t) = a(x,t), \quad (x,t) \in \mathfrak{Q}^-, \quad \text{ensuring} \quad a_1(x,t) < 0, (x,t) \in \mathfrak{Q}, \\
&a_2(x,t) = a(x,t), \quad (x,t) \in \mathfrak{Q}^+, \quad \text{ensuring} \quad a_1(x,t) > 0, (x,t) \in \mathfrak{Q}.
\end{aligned}$$

Examine the functions

$$u(x,t) = \begin{cases} u_1(x,t) + \left(u(0,t) - u_1(0,1)\right)\Xi_1(x,t) + \Lambda_1 \Xi_2(x,t), & (x,t) \in \mathfrak{Q}^-, \\ u_2(x,t) + \Lambda_2 \Xi_1(x,t) + \left(u(1,t) - u_2(0,1)\right)\Xi_2(x,t), & (x,t) \in \mathfrak{Q}^+, \end{cases}$$

where $\Xi_1(x,t), \Xi_2(x,t)$ are solutions of resulting TP-SPPs:

$$\begin{aligned}
&\left(\varepsilon \Xi_{1xx} + \mu a_1 \Xi_{1x} - b\Xi_1 - c\Xi_{1t}\right)(x,t) = 0, \Xi_1(0,t) = 1, \Xi_1(1,t) = 0, \Xi_1(x,0) = 0, \\
&\left(\varepsilon \Xi_{2xx} + \mu a_2 \Xi_{2x} - b\Xi_2 - c\Xi_{2t}\right)(x,t) = 0, \Xi_2(0,t) = 0, \Xi_2(1,t) = 1, \Xi_2(x,0) = 0.
\end{aligned}$$

Observe that $u(x,t)$ satisfies Eq. (1.1) in $\mathfrak{Q}^- \cup \mathfrak{Q}^+$ with two well-chosen constants Λ_1, Λ_2, so that $u(x,t) \in C^1(\mathfrak{Q})$. On $(0,1), 0 < \Xi_i(x,t) < 1, i = 1,2$ on $\mathfrak{Q}$ [4, 10]. Thus, $\Xi_1(x,t), \Xi_2(x,t)$ is unable to reach extremum at interior points of the domain, and as a result, $\Xi_1^{'}(x,t) < 0, \Xi_2^{'}(x,t) > 0, (x,t) \in \mathfrak{Q}$. Next, we apply $u(\varphi-,t) = u(\varphi+,t)$ and $u^{'}(\varphi-,t) = u^{'}(\varphi+,t)$. Now, we require relation for existence of Λ_1, Λ_2,

$$\begin{vmatrix} \Xi_2(\varphi,t) & -\Xi_1(\varphi,t) \\ \Xi_2^{'}(\varphi,t) & -\Xi_1^{'}(\varphi,t) \end{vmatrix} = \Xi_2^{'}(\varphi,t)\Xi_1(\varphi,t) - \Xi_2(\varphi,t)\Xi_1^{'}(\varphi,t) > 0.$$

□

The operator $\Phi_{\varepsilon,\mu}$ of Eq. (1.1) follows the maximum principle outlined on $\overline{\mathfrak{Q}}$.

Lemma 2.2. *(Comparison Principle) If* $\mathfrak{F} \in C^{(0)}(\overline{\mathfrak{Q}}) \cap C^{(1)}(\mathfrak{Q}) \cap C^{(2)}(\mathfrak{Q}^- \cup \mathfrak{Q}^+)$ *such that* $\mathfrak{F}(0,t) \geq 0, \mathfrak{F}(x,0) \geq 0, \mathfrak{F}(1,t) \geq 0, \left[\mathfrak{F}^{'}\right](\varphi,t) = \left[\mathfrak{F}^{'}\right](\varphi+,t) - \left[\mathfrak{F}^{'}\right](\varphi-,t) \geq 0$, *and* $\Phi_{\varepsilon,\mu}\mathfrak{F}(x,t) \geq 0, \forall (x,t) \in \mathfrak{Q}$, *then* $\mathfrak{F}(x,t) \leq 0, \forall (x,t) \in \overline{\mathfrak{Q}}$.

Proof. Suppose the function ν defined on $\overline{\mathfrak{Q}}$ be such that

$$\mathfrak{F}(x,t) = \exp\left(-\alpha\mu\left|x-\varphi\right|/2\varepsilon\right)\nu(x,t), \quad \alpha = \min\left\{\alpha_1, \alpha_2\right\}.$$

We presume that ν attains its peak value at $(\varsigma,\tau) \in \overline{\mathfrak{Q}}$ and $\nu(\varsigma,\tau) > 0$. According to the maximum principle assumption, (ς,τ) is either in $(\mathfrak{Q}^- \cup \mathfrak{Q}^+)$ or it is $(\varsigma,\tau) = (\varphi,\tau)$. Thus, we have three scenarios to consider:

(1) If $(\varsigma,\tau)\in\mathfrak{Q}^-$, then

$$\Phi_{\varepsilon,\mu}\mathfrak{F}(\varsigma,\tau)=e^{(-\alpha_1\mu(\varphi-\varsigma)/2\varepsilon)}\left(\varepsilon\frac{\partial^2\nu}{\partial x^2}+\mu(\alpha_1+a)\frac{\partial\nu}{\partial x}+\left(\frac{\alpha_1\mu^2}{2\varepsilon}\left(\frac{\alpha_1}{2}+a\right)-b\right)\nu-c\frac{\partial\nu}{\partial t}\right)(\varsigma,\tau)<0,$$

(2) If $(\varsigma,\tau)\in\mathfrak{Q}^+$, then

$$\Phi_{\varepsilon,\mu}\mathfrak{F}(\varsigma,\tau)=e^{(-\alpha_2\mu(\varsigma-\varphi)/2\varepsilon)}\left(\varepsilon\frac{\partial^2\nu}{\partial x^2}+\mu(a-\alpha_2)\frac{\partial\nu}{\partial x}+\left(\frac{\alpha_2\mu^2}{2\varepsilon}\left(\frac{\alpha_2}{2}-a\right)-b\right)\nu-c\frac{\partial\nu}{\partial t}\right)(\varsigma,\tau)<0,$$

From step (1) and (2), we have contradiction to hypothesis that $\Phi_{\varepsilon,\mu}\mathfrak{F}(x,t)\geq 0,(x,t)\in(\mathfrak{Q}^-\cup\mathfrak{Q}^+)$.

(3) If $(\varsigma,\tau)=(\varphi,\tau)$, then we have

$$\left[\frac{\partial\mathfrak{F}}{\partial x}\right](\varphi,\tau)=\left[\frac{\partial\nu}{\partial x}\right](\varphi,\tau)-\left(\frac{\alpha_1+\alpha_2}{2\varepsilon}\right)\nu(\varphi,\tau),$$

and since, we assume that ν has a maximum at (φ,τ), it shows that $\left[\frac{\partial\mathfrak{F}}{\partial x}\right](\varphi,\tau)\leq 0$, which is also a contradiction.

□

Thus, we arrive at the subsequent lemma, showing that the solution is stable.

Lemma 2.3. *(Stability Result). The bounds for $u(x,t)$ of Eq. (1.1) are as follows:*

$$\|u\|_{\overline{\mathfrak{Q}}}\leq C\max\left\{\|\vartheta\|_{\mathfrak{Q}_l},\|\xi\|_{\mathfrak{Q}_r},\|\phi\|_{\mathfrak{Q}_b}\right\}+\frac{1}{\mathfrak{K}}\|\Phi_{\varepsilon,\mu}u\|_{(\mathfrak{Q}^-\cup\mathfrak{Q}^+)},\tag{2.1}$$

where $\mathfrak{K}=\min\left\{\frac{\alpha_1}{\varphi},\frac{\alpha_2}{1-\varphi}\right\}$.

Proof. See [2, 19] for the proof. □

Lemma 2.4. *Let* $\alpha=\min\{\alpha_1,\alpha_2\}$ *and* $\mathfrak{B}=\min_{\mathfrak{Q}^-\cup\mathfrak{Q}^+}\left\{\frac{b(x,t)}{a(x,t)}\right\}$. *For* $1\leq\kappa+2\iota\leq 3$, *then the solution* $u(x,t)$ *of Eq. (1.1) and its derivatives satisfy:*

(1) *If* $\alpha\mu^2\leq\mathfrak{B}\varepsilon$, *then*

$$\left\|\frac{\partial^{\kappa+\iota}u}{\partial x^\kappa\partial t^\iota}\right\|_{\mathfrak{Q}^-\cup\mathfrak{Q}^+}\leq\frac{C}{(\sqrt{\varepsilon})^\kappa}\max\left\{\|u\|_{\overline{\mathfrak{Q}}},\sum_{i+2j=0}^{2}(\sqrt{\varepsilon})^i\left\|\frac{\partial^{i+j}\varpi}{\partial x^i\partial t^j}\right\|,\sum_{i=0}^{4}\left[(\sqrt{\varepsilon})^i\left\|\frac{d^i\phi}{dx^i}\right\|_{\mathfrak{Q}_b}+\left\|\frac{d^i\vartheta}{dt^i}\right\|_{\mathfrak{Q}_l}+\left\|\frac{d^i\xi}{dt^i}\right\|_{\mathfrak{Q}_r}\right]\right\},$$

(2) $\alpha\mu^2\geq\mathfrak{B}\varepsilon$, *then*

$$\left\|\frac{\partial^{\kappa+\iota}u}{\partial x^\kappa\partial t^\iota}\right\|_{\mathfrak{Q}^-\cup\mathfrak{Q}^+}\leq C\left(\frac{\mu}{\varepsilon}\right)^\kappa\left(\frac{\mu^2}{\varepsilon}\right)^\iota\max\left\{\|u\|_{\overline{\mathfrak{Q}}},\sum_{i+2j=0}^{2}\frac{\varepsilon^{i+j+1}}{\mu^{i+2j+2}}\left\|\frac{\partial^{i+j}\varpi}{\partial x^i\partial t^j}\right\|,\sum_{i=0}^{4}\left[\left(\frac{\varepsilon}{\mu}\right)^i\left\|\frac{d^i\phi}{dx^i}\right\|_{\mathfrak{Q}_b}+\left\|\frac{d^i\vartheta}{dt^i}\right\|_{\mathfrak{Q}_l}+\left\|\frac{d^i\xi}{dt^i}\right\|_{\mathfrak{Q}_r}\right]\right\},$$

where C depends only on the coefficients and their derivatives.

Proof. See [2] for the proof □

Corollary 2.5. *Assuming initial data of Eq. (1.1) is sufficiently smooth, the solution's second time derivative meets the following bound [3]:* $\|u_{tt}\|_{(\mathfrak{Q}^-\cup\mathfrak{Q}^+)}=\begin{cases}C, & \text{if } \alpha\mu^2\leq\mathfrak{B}\varepsilon,\\ C\mu^4\varepsilon^{-2}, & \text{if } \alpha\mu^2\geq\mathfrak{B}\varepsilon.\end{cases}$

3. Discrete Problem and Numerical Scheme

3.1. **Temporal Discretization.** This section presents a numerical scheme using Implicit Euler method to solve Eq. (1.1). A uniform mesh $\Omega^M = \{t_j = jk, j = 0(1)M, k = T/M\}$ is created by dividing time interval into M equal parts for a fixed T. Now, on $\mathfrak{Q}^{\varphi} = (\mathfrak{Q}^- \cup \mathfrak{Q}^+) \times \Omega^M$, Eq. (1.1) is semi-discretized as:

$$\begin{aligned}
&\varepsilon \left(U_{xx}\right)^{j+1}(x) + \mu a^{j+1}(x) \left(U_x\right)^{j+1}(x) - \left(b^{j+1}(x) + \frac{c^{j+1}(x)}{k}\right) U^{j+1}(x) = \varpi^{j+1}(x) - \frac{c^j(x)}{k} U^j(x), j = 0(1)M-1,\\
&U^{j+1}(0) = \vartheta(t_{j+1}), \quad U^{j+1}(1) = \xi(t_{j+1}), 0 \le j \le M, \qquad (3.1)\\
&U^0(x) = \phi(x), x \in \Omega,
\end{aligned}$$

where $U^{j+1}(x)$ is the approximation of $u(x, t_{j+1})$. Rewrite Eq. (3.1) as:

$$\begin{cases}
\Phi^M_{\varepsilon,\mu} U^{j+1}(x) = z(x, t_{j+1}), x \in \mathfrak{Q}^{\varphi}, & 0 \le j \le M-1,\\
U^{j+1}(0) = \vartheta(t_{j+1}), \quad U^{j+1}(1) = \xi(t_{j+1}), & 0 \le j \le M,\\
U^0(x) = \phi(x), & x \in \Omega,
\end{cases} \qquad (3.2)$$

where $\Phi^M_{\varepsilon,\mu} U^{j+1}(x) = \varepsilon \left(U_{xx}\right)^{j+1}(x) + \mu a^{j+1}(x) \left(U_x\right)^{j+1}(x) - \left(b^{j+1}(x) + \frac{c^{j+1}(x)}{k}\right) U^{j+1}(x)$, and $z(x, t_{j+1}) = \varpi^{j+1}(x) - \frac{c^j(x)}{k} U^j(x)$. The operator $\Phi^M_{\varepsilon,\mu}$ complies with semi-discrete maximum rule outlined below:

Lemma 3.1. *(Maximum principle in a semi-discrete form) Let $\mathfrak{F}(x, t_{j+1})$ be a smooth function satisfies $\mathfrak{F}(x, t_{j+1}) \ge 0$ for $x = 0, 1$, $\left[\mathfrak{F}'\right](\varphi, t_{j+1}) = \mathfrak{F}'(\varphi+, t_{j+1}) - \mathfrak{F}'(\varphi-, t_{j+1}) \ge 0$, and $\Phi^M_{\varepsilon,\mu} \mathfrak{F}(x, t_{j+1}) \ge 0, \forall x \in (0, 1)$, then $\mathfrak{F}(x, t_{j+1}) \le 0, \forall x \in [0, 1]$.*

Proof. See [9] for the proof of this lemma. □

Lemma 3.2. *Let $\mathfrak{E}_{j+1} = U^{j+1}(x) - u(x, t_{j+1})$ be the local truncation error($\mathcal{LTE}$) at $(j+1)$th time step. Then $\|\mathfrak{E}_{j+1}\|_\infty \le C(k^2)$ for constant C. Moreover, if $\mathcal{E}_j = u(x, t_j) - U(x, t_j)$ denotes global error in the time direction. Consequently, it can be concluded that*

$$\|\mathcal{E}_{j+1}\|_\infty = \left\| \sum_{k=1}^{j} \mathfrak{E}_k \right\| = \|\mathfrak{E}_1\|_\infty + \ldots + \|\mathfrak{E}_j\|_\infty \le C(k).$$

Lemma 3.3. *Let $U^{j+1}(x)$ be the solution of Eq. (3.2). Then*

$$\left|U^{j+1}(x)\right| \le \max\left\{ \left|U(0, t_{j+1})\right|, \left|U(1, t_{j+1})\right|, \frac{\|\varpi\|}{\mathfrak{K}} \right\}, \quad \forall x \in [0, 1]. \qquad (3.3)$$

Proof. Defining the barrier function as

$$\Xi^{\pm}(x, t_{j+1}) = \mathcal{W} \pm U^{j+1}(x), \quad \text{where} \quad \mathcal{W} = \max\left\{ \left|U(0, t_{j+1})\right|, \left|U(1, t_{j+1})\right|, \frac{\|\varpi\|}{\mathfrak{K}} \right\}.$$

Then, we have $\Xi^{\pm}(0, t_{j+1}) \ge 0$ and $\Xi^{\pm}(1, t_{j+1}) \ge 0$. Now, consider the two cases:

(1) For $x \in \mathfrak{Q}^-$, i.e., $x \in [0, \varphi]$, we have:

$$\Phi^M_{\varepsilon,\mu} \Xi^{\pm}(x, t_{j+1}) = -\left(b^{j+1}(x) + \frac{c^{j+1}(x)}{k}\right) \mathcal{W} \pm \Phi^M_{\varepsilon,\mu} U(x, t_{j+1}) < 0,$$

since, $\left(b^{j+1}(x) + \frac{c^{j+1}(x)}{k}\right) > 0$.

(2) For $x \in \mathfrak{Q}^+$, i.e., $x \in [\varphi, 1]$, we have:

$$\Phi^M_{\varepsilon,\mu} \Xi^{\pm}(x, t_{j+1}) = -\left(b^{j+1}(x) + \frac{c^{j+1}(x)}{k}\right) \mathcal{W} \pm \Phi^M_{\varepsilon,\mu} U(x, t_{j+1}) < 0,$$

since, $\left(b^{j+1}(x)+\frac{c^{j+1}(x)}{k}\right)>0.$

As a result of the preceding lemma, the desired conclusion is obtained □

3.2. **Spatial Semi-Discretization and Non-Polynomial Cubic Spline Approach.** We employed a non-polynomial cubic spline in the compression method outlined below to approximate Eq. (3.2). Let $x_0=0, x_N=1, x_i=ih$, where h is the mesh length and N is the number of subintervals in spatial domain. In (x_i, x_{i+1}), the function $\mathcal{A}^{j+1}(x,\theta)\in C^2[0,1]$ interpolates $U^{j+1}(x_i)=U(x_i,t_{j+1})$ at the mesh points $x_i, i=0(1)N$ and depends on a parameter $\theta>0$. As $\theta\to 0$, this function reduces to cubic spline on $[0,1]$, and is known as a parameteric cubic spline function. In (x_i,x_{i+1}), $\mathcal{A}^{j+1}(x,\theta)=\mathcal{A}^{j+1}(x)$ satisfies the following differential equation:

$$\begin{aligned}\frac{d^2\mathcal{A}^{j+1}(x_i)}{dx^2}+\theta\mathcal{A}^{j+1}(x_i)&=\left(\frac{x_{i+1}-x}{h}\right)\left[\frac{d^2\mathcal{A}^{j+1}(x_i)}{dx^2}+\theta\mathcal{A}^{j+1}(x_i)\right]\\&+\left(\frac{x-x_i}{h}\right)\left[\frac{d^2\mathcal{A}^{j+1}(x_{i+1})}{dx^2}+\theta\mathcal{A}^{j+1}(x_{i+1})\right],\end{aligned}\tag{3.4}$$

where $\mathcal{A}^{j+1}(x_i)=U^{j+1}(x_i)$ and $\theta>0$ is called a cubic spline under compression. Solving Eq. (3.4) and finding the arbitrary constants using interpolation conditions $\mathcal{A}^{j+1}(x_{i+1})=U^{j+1}(x_{i+1}), \mathcal{A}^{j+1}(x_i)=U^{j+1}(x_i)$ and after writing $\lambda=h\theta^{\frac{1}{2}}$:

$$\begin{aligned}\mathcal{A}^{j+1}(x)=&-\frac{h^2}{\lambda^2\sin\lambda}\left[\mathfrak{M}_{i+1}\sin\left(\frac{\lambda(x-x_i)}{h}\right)+\mathfrak{M}_i\sin\left(\frac{\lambda(x_{i+1}-x)}{h}\right)\right]\\&+\frac{h^2}{\lambda^2}\left[\left(\frac{x-x_i}{h}\right)\left(\mathfrak{M}_{i+1}+\frac{\lambda^2}{h^2}\mathcal{A}^{j+1}(x_{i+1})\right)+\left(\frac{x_{i+1}-x}{h}\right)\left(\mathfrak{M}_i+\frac{\lambda^2}{h^2}\mathcal{A}^{j+1}(x_i)\right)\right],\end{aligned}\tag{3.5}$$

Differentating Eq. (3.5) and letting $x\to x_i$, we have

$$\frac{\mathcal{A}^{j+1}(x_i+)}{dx}=\frac{U^{j+1}(x_{i+1})-U^{j+1}(x_i)}{h}+\frac{h}{\lambda^2}\left[\left(1-\frac{\lambda}{\sin\lambda}\right)\mathfrak{M}_{i+1}-(1-\lambda\cot\lambda)\mathfrak{M}_i\right],\tag{3.6}$$

By analyzing the interval (x_{i-1},x_i) and following the same steps, we obtain:

$$\frac{\mathcal{A}^{j+1}(x_i-)}{dx}=\frac{U^{j+1}(x_i)-U^{j+1}(x_{i-1})}{h}+\frac{h}{\lambda^2}\left[(1-\lambda\cot\lambda)\mathfrak{M}_i-\left(1-\frac{\lambda}{\sin\lambda}\right)\mathfrak{M}_{i-1}\right],\tag{3.7}$$

By setting Eq. (3.6) equal to Eq. (3.7) at x_i, we get

$$\begin{aligned}&\frac{U^{j+1}(x_i)-U^{j+1}(x_{i-1})}{h}+\frac{h}{\lambda^2}\left[(1-\lambda\cot\lambda)\mathfrak{M}_i-\left(1-\frac{\lambda}{\sin\lambda}\right)\mathfrak{M}_{i-1}\right]\\&=\frac{U^{j+1}(x_{i+1})-U^{j+1}(x_i)}{h}+\frac{h}{\lambda^2}\left[\left(1-\frac{\lambda}{\sin\lambda}\right)\mathfrak{M}_{i+1}-(1-\lambda\cot\lambda)\mathfrak{M}_i\right],\end{aligned}\tag{3.8}$$

Next, Eq. (3.8) results in a tridiagonal system

$$h^2\left(\lambda_1\mathfrak{M}_{i-1}+2\lambda_2\mathfrak{M}_i+\lambda_1\mathfrak{M}_{i+1}\right)=U_{i-1}^{j+1}-2U_i^{j+1}+U_{i+1}^{j+1},\tag{3.9}$$

where $\lambda_1=\frac{1}{\lambda^2}\left(\frac{\lambda}{\sin\lambda}-1\right), \lambda_2=\frac{1}{\lambda^2}(1-\lambda\cot\lambda), \mathfrak{M}_i=\frac{d^2\mathcal{A}^{j+1}(x_i)}{dx^2}$ and $\lambda_1+\lambda_2=\frac{1}{2}, i=1(1)N-1$. The continuity condition provided by Eq. (3.9) guarantees the smoothness of the first-order derivatives of spline $\mathcal{A}^{j+1}(x,\theta)$ at the interior nodes. Eq. (3.2) at $x=x_q, q=i-1,i,i+1$ can be expressed as:

$$\varepsilon\mathfrak{M}_q=-\mu a^{j+1}(x_q)\left(U_x(x_q)\right)^{j+1}+\left(b^{j+1}(x_q)+\frac{c^{j+1}(x_q)}{k}\right)U^{j+1}(x_q)+\mathcal{R}^{j+1}(x_q),\tag{3.10}$$

where $\mathcal{R}^{j+1}(x_q) = \varpi^{j+1}(x_q) - \frac{c^j(x_q)}{k} U^j(x_q)$. Now, Eq. (3.10) at $q = i, i \pm 1$, becomes:

$$\begin{cases} \varepsilon \mathfrak{M}_i = -\mu a^{j+1}(x_i) \left(U_x(x_i)\right)^{j+1} + \left(b^{j+1}(x_i) + \frac{c^{j+1}(x_i)}{k}\right) U^{j+1}(x_i) + \mathcal{R}^{j+1}(x_i), \\ \varepsilon \mathfrak{M}_{i-1} = -\mu a^{j+1}(x_{i-1}) \left(U_x(x_{i-1})\right)^{j+1} + \left(b^{j+1}(x_{i-1}) + \frac{c^{j+1}(x_{i-1})}{k}\right) U^{j+1}(x_{i-1}) + \mathcal{R}^{j+1}(x_{i-1}), \\ \varepsilon \mathfrak{M}_{i+1} = -\mu a^{j+1}(x_{i+1}) \left(U_x(x_{i+1})\right)^{j+1} + \left(b^{j+1}(x_{i+1}) + \frac{c^{j+1}(x_{i+1})}{k}\right) U^{j+1}(x_{i+1}) + \mathcal{R}^{j+1}(x_{i+1}). \end{cases} \tag{3.11}$$

Now, we apply finite difference approximation to approximate $\frac{dU^{j+1}(x_q)}{dx}$ in Eq. (3.11):

$$\begin{cases} \frac{dU^{j+1}(x_{i-1})}{dx} \approx \dfrac{-U_{i+1}^{j+1} + 4U_i^{j+1} - 3U_{i-1}^{j+1}}{2h}, \\ \frac{dU^{j+1}(x_i)}{dx} \approx \dfrac{U_{i+1}^{j+1} - U_{i-1}^{j+1}}{2h}, \\ \frac{dU^{j+1}(x_{i+1})}{dx} \approx \dfrac{3U_{i+1}^{j+1} - 4U_i^{j+1} + U_{i-1}^{j+1}}{2h}. \end{cases} \tag{3.12}$$

Now, using Eq. (3.12), Eq. (3.11) reduced to:

$$\begin{cases} \varepsilon \mathfrak{M}_i = \frac{\mu}{2h} a_i^{j+1} U_{i-1}^{j+1} + \left(b_i^{j+1} + \frac{c_i^{j+1}}{k}\right) U_i^{j+1} - \frac{\mu}{2h} a_i^{j+1} U_{i+1}^{j+1} + \mathcal{R}_i^{j+1}, \\ \varepsilon \mathfrak{M}_{i-1} = \left[\frac{3\mu}{2h} a_{i-1}^{j+1} + \left(b_{i-1}^{j+1} + \frac{c_{i-1}^{j+1}}{k}\right)\right] U_{i-1}^{j+1} - \frac{2\mu}{h} a_{i-1}^{j+1} U_i^{j+1} + \frac{\mu}{2h} a_{i-1}^{j+1} U_{i+1}^{j+1} + \mathcal{R}_{i-1}^{j+1}, \\ \varepsilon \mathfrak{M}_{i+1} = -\frac{\mu}{2h} a_{i+1}^{j+1} U_{i-1}^{j+1} + \frac{2\mu}{h} a_{i+1}^{j+1} U_i^{j+1} + \left[-\frac{3\mu}{2h} a_{i+1}^{j+1} + \left(b_{i+1}^{j+1} + \frac{c_{i+1}^{j+1}}{k}\right)\right] U_{i+1}^{j+1} + \mathcal{R}_{i+1}^{j+1}. \end{cases} \tag{3.13}$$

By replacing Eq. (3.13) into Eq. (3.9), we obtain

$$\begin{aligned} &\left[-\frac{\varepsilon}{h^2} + \frac{3\lambda_1}{2h}\mu a_{i-1}^{j+1} + \frac{\lambda_2}{h}\mu a_i^{j+1} - \frac{\lambda_1}{2h}\mu a_{i+1}^{j+1} + \lambda_1\left(b_{i-1}^{j+1} + \frac{c_{i-1}^{j+1}}{k}\right)\right] U_{i-1}^{j+1} \\ &+ \left[\frac{2\varepsilon}{h^2} - \frac{2\lambda_1}{h}\mu a_{i-1}^{j+1} + \frac{2\lambda_1}{h}\mu a_{i+1}^{j+1} + 2\lambda_2\left(b_i^{j+1} + \frac{c_i^{j+1}}{k}\right)\right] U_i^{j+1} \\ &+ \left[-\frac{\varepsilon}{h^2} + \frac{\lambda_1}{2h}\mu a_{i-1}^{j+1} - \frac{\lambda_2}{h}\mu a_i^{j+1} - \frac{3\lambda_1}{2h}\mu a_{i+1}^{j+1} + \lambda_1\left(b_{i+1}^{j+1} + \frac{c_{i+1}^{j+1}}{k}\right)\right] U_{i+1}^{j+1} \\ &= -\left[\lambda_1 \varpi_{i-1}^{j+1} + 2\lambda_2 \varpi_i^{j+1} + \lambda_1 \varpi_{i+1}^{j+1}\right] + \lambda_1 \frac{c_{i-1}^j}{k} U_{i-1}^j + 2\lambda_2 \frac{c_i^j}{k} U_i^j + \lambda_1 \frac{c_{i+1}^j}{k} U_{i+1}^j. \end{aligned} \tag{3.14}$$

Upon multiplying the terms in Eq. (3.14) that contain $\varepsilon\ \delta(\rho)$, we obtain

$$\begin{aligned} &\left[-\frac{\delta(\rho)\varepsilon}{h^2} + \frac{3\lambda_1}{2h}\mu a_{i-1}^{j+1} + \frac{\lambda_2}{h}\mu a_i^{j+1} - \frac{\lambda_1}{2h}\mu a_{i+1}^{j+1} + \lambda_1\left(b_{i-1}^{j+1} + \frac{c_{i-1}^{j+1}}{k}\right)\right] U_{i-1}^{j+1} \\ &+ \left[\frac{2\delta(\rho)\varepsilon}{h^2} - \frac{2\lambda_1}{h}\mu a_{i-1}^{j+1} + \frac{2\lambda_1}{h}\mu a_{i+1}^{j+1} + 2\lambda_2\left(b_i^{j+1} + \frac{c_i^{j+1}}{k}\right)\right] U_i^{j+1} \\ &+ \left[-\frac{\delta(\rho)\varepsilon}{h^2} + \frac{\lambda_1}{2h}\mu a_{i-1}^{j+1} - \frac{\lambda_2}{h}\mu a_i^{j+1} - \frac{3\lambda_1}{2h}\mu a_{i+1}^{j+1} + \lambda_1\left(b_{i+1}^{j+1} + \frac{c_{i+1}^{j+1}}{k}\right)\right] U_{i+1}^{j+1} \\ &= -\lambda_1\left[\varpi_{i-1}^{j+1} - \frac{c_{i-1}^j}{k} U_{i-1}^j\right] - 2\lambda_2\left[\varpi_{i-1}^{j+1} - \frac{c_i^j}{k} U_i^j\right] - \lambda_1\left[\varpi_{i+1}^{j+1} - \frac{c_{i+1}^j}{k} U_{i+1}^j\right] \end{aligned} \tag{3.15}$$

It is necessary to evaluate the fitting factor $\delta(\rho)$ so that the solution of Eq. (3.15) converges uniformly to Eq. (1.1). At the moment, the three-term recurrence relation for Eq. (3.15) is written as:

$$\begin{aligned}
&\Phi_{\varepsilon,\mu}^{N,M} U_i^{j+1} \equiv \mathfrak{Y}_i^{-} U_{i-1}^{j+1} + \mathfrak{Y}_i^{c} U_i^{j+1} + \mathfrak{Y}_i^{+} U_{i+1}^{j+1} = \mathcal{H}_i^j, \\
&U^{j+1}(0) = \vartheta^{j+1}(0), \quad U^{j+1}(1) = \xi^{j+1}(1), \quad 0 \le j \le M, \\
&U_i^0 = \phi(x_i), \quad x \in [0,1],
\end{aligned} \tag{3.16}$$

$i = 1(1)N-1, j = 1(1)M-1$, where

$$\begin{cases}
\mathfrak{Y}^{-} = -\dfrac{\delta(\rho)\varepsilon}{h^2} + \dfrac{3\lambda_1}{2h}\mu a_{i-1}^{j+1} + \dfrac{\lambda_2}{h}\mu a_i^{j+1} - \dfrac{\lambda_1}{2h}\mu a_{i+1}^{j+1} + \lambda_1\left(b_{i-1}^{j+1} + \frac{c_{i-1}^{j+1}}{k}\right), \\
\mathfrak{Y}^{c} = \dfrac{2\delta(\rho)\varepsilon}{h^2} - \dfrac{2\lambda_1}{h}\mu a_{i-1}^{j+1} + \dfrac{2\lambda_1}{h}\mu a_{i+1}^{j+1} + 2\lambda_2\left(b_i^{j+1} + \frac{c_i^{j+1}}{k}\right), \\
\mathfrak{Y}^{+} = -\dfrac{\delta(\rho)\varepsilon}{h^2} + \dfrac{\lambda_1}{2h}\mu a_{i-1}^{j+1} - \dfrac{\lambda_2}{h}\mu a_i^{j+1} - \dfrac{3\lambda_1}{2h}\mu a_{i+1}^{j+1} + \lambda_1\left(b_{i+1}^{j+1} + \frac{c_{i+1}^{j+1}}{k}\right), \\
\mathcal{H}_i^j = -\lambda_1\left[\varpi_{i-1}^{j+1} - \frac{c_{i-1}^j}{k}U_{i-1}^j\right] - 2\lambda_2\left[\varpi_{i-1}^{j+1} - \frac{c_i^j}{k}U_i^j\right] - \lambda_1\left[\varpi_{i+1}^{j+1} - \frac{c_{i+1}^j}{k}U_{i+1}^j\right].
\end{cases} \tag{3.17}$$

The points on the line $(x_{N/2}, t_{j+1})$ are found in the region $\mathfrak{M}^{N\pm} = \mathfrak{M}^{\pm} \cap \mathfrak{Q}^N$ as shown in Figure 1. To tackle the discontinuity point $(x_{N/2}, t_{j+1}) = (\varphi, t_{j+1})$, we used a second order hybrid difference operator as:

$$\Phi_{\varepsilon,\mu}^{N,M} U_{\frac{N}{2}}^{j+1} = \frac{-U_{\frac{N}{2}+2}^{j+1} + 4U_{\frac{N}{2}+1}^{j+1} - 3U_{\frac{N}{2}}^{j+1}}{2h} - \frac{U_{\frac{N}{2}-2}^{j+1} - 4U_{\frac{N}{2}-1}^{j+1} + 3U_{\frac{N}{2}}^{j+1}}{2h} = 0. \tag{3.18}$$

Tri-diagonal systems, when combined with exponential fitting factors, have been shown to provide uniform convergence, which is critical for accurately capturing sharp gradients and discontinuities.

3.3. **Determining the fitting factor.** To ensure that Eq. (3.16) uniformly converges to the solution of Eq. (1.1), it is essential to determine the fitting factor($\delta(\rho)$). Given that the fitting factor is time-independent, Eq. (3.15) can be reformulated to solve for $\delta(\rho)$ in Eq. (3.16).

$$\begin{aligned}
&-\frac{\delta(\rho)\varepsilon}{h^2}\left[U_{i-1}^{j+1} - 2U_i^{j+1} + U_{i+1}^{j+1}\right] + \left[\frac{3\lambda_1}{2h}\mu a_{i-1}^{j+1} + \frac{\lambda_2}{h}\mu a_i^{j+1} - \frac{\lambda_1}{2h}\mu a_{i+1}^{j+1} + \lambda_1\left(b_{i-1}^{j+1} + \frac{c_{i-1}^{j+1}}{k}\right)\right]U_{i-1}^{j+1} \\
&+\left[-\frac{2\lambda_1}{h}\mu a_{i-1}^{j+1} + \frac{2\lambda_1}{h}\mu a_{i+1}^{j+1} + 2\lambda_2\left(b_i^{j+1} + \frac{c_i^{j+1}}{k}\right)\right]U_i^{j+1} \\
&+\left[\frac{\lambda_1}{2h}\mu a_{i-1}^{j+1} - \frac{\lambda_2}{h}\mu a_i^{j+1} - \frac{3\lambda_1}{2h}\mu a_{i+1}^{j+1} + \lambda_1\left(b_{i+1}^{j+1} + \frac{c_{i+1}^{j+1}}{k}\right)\right]U_{i+1}^{j+1} = \mathcal{H}_i^j.
\end{aligned} \tag{3.19}$$

By Multiplying both sides of Eq. (3.19) by h and considering $\lim_{h\to 0}$, we obtain:

$$-\frac{\delta(\rho)}{\rho}\left[U_{i-1}^{j+1} - 2U_i^{j+1} + U_{i+1}^{j+1}\right] + \mu a_0\left(\lambda_1 + \lambda_2\right)\left[U_{i-1}^{j+1} - U_{i+1}^{j+1}\right] = 0, \tag{3.20}$$

where $\rho = h/\varepsilon$. When the boundary layer is on the left side of the domain, from the theory of singular perturbation [23], the solution of Eq. (3.2) is of the form:

$$U^{j+1}(x) = U_0^{j+1}(x) + \frac{a^{j+1}(0)}{a^{j+1}(x)}\left(\vartheta^{j+1}(0) - U_0^{j+1}(0)\right)e^{\left(-\int_0^x\left(-\frac{\mu a^{j+1}(x)}{\varepsilon}\right)dx\right)}, \tag{3.21}$$

where $U_0^{j+1}(x)$ is solution of the reduced problem of Eq. (3.2). By limiting the Taylor series expansion of $a^{j+1}(x)$ to its first term around $x = 0$ and then taking the limit as $h \to 0$, we end up with:

$$\lim_{h\to 0} U^{j+1}(ih) = U_0^{j+1}(0) + \left(\vartheta^{j+1}(0) - U_0^{j+1}(0)\right)e^{\left(-a^{j+1}(0)\mu\left(\frac{1}{\varepsilon} - i\rho\right)\right)} + O(\varepsilon). \tag{3.22}$$

Substituting Eq. (3.22) into Eq. (3.20) and simplifying provides the fitting factor as:

$$\delta_0(\rho) = \rho\mu(\lambda_1+\lambda_2)a^{j+1}(0)\coth\left(\frac{\rho\mu a^{j+1}(0)}{2}\right). \tag{3.23}$$

When a boundary layer develops along the right boundary of the region, the outcome is:

$$U^{j+1}(x) = U_0^{j+1}(x) + \frac{a^{j+1}(1)}{a^{j+1}(x)}\left(\xi^{j+1}(1) - U_0^{j+1}(1)\right)e^{\left(-\int_x^1\left(-\frac{\mu a^{j+1}(x)}{\varepsilon}\right)dx\right)}. \tag{3.24}$$

By applying Taylor series expansion to $a^{j+1}(x)$ and limiting it to the first term about $x=1$ in Eq. (3.24), while also considering the limit as $h\to 0$, we arrive at :

$$\lim_{h\to 0} U^{j+1}(ih) = U_0^{j+1}(1) + \left(\xi^{j+1}(1) - U_0^{j+1}(1)\right)e^{\left(-a^{j+1}(1)\mu\left(\frac{1}{\varepsilon}-i\rho\right)\right)} + O(\varepsilon). \tag{3.25}$$

After making adjustments and substituting Eq. (3.25) into Eq (3.20), we obtain

$$\delta_1(\rho) = \rho\mu(\lambda_1+\lambda_2)a^{j+1}(N)\coth\left(\frac{\rho\mu a^{j+1}(N)}{2}\right). \tag{3.26}$$

Consequently, a variable fitting factor with discontinuous convection coefficient $a(x,t)$ is obtained from the data in Eqs. (3.26), (3.23) and is given as

$$\delta_\varphi(\rho) = \begin{cases} \rho\mu(\lambda_1+\lambda_2)a_1^{j+1}(i)\coth\left(\frac{\rho\mu a_1^{j+1}(i)}{2}\right), & \text{if } 0\le i\le N/2, \\ \rho\mu(\lambda_1+\lambda_2)a_2^{j+1}(i)\coth\left(\frac{\rho\mu a_2^{j+1}(i)}{2}\right), & \text{if } N/2\le i<N. \end{cases} \tag{3.27}$$

4. Convergence Analysis

Before presenting the main results regarding the convergence of the suggested scheme, we outline some essential properties fulfilled by $\Phi_{\varepsilon,\mu}^{N,M}$.

Lemma 4.1. *(Discrete Comparison Principle) Let $\mathbb{W}_i^{j+1}$ be a comparison function such that if $U_0^{j+1}\le\mathbb{W}_0^{j+1}$ and $U_N^{j+1}\le\mathbb{W}_N^{j+1}$, then $\Phi_{\varepsilon,\mu}^{N,M}U_i^{j+1}\le\Phi_{\varepsilon,\mu}^{N,M}\mathbb{W}_i^{j+1}, i=1(1)N-1$ implies that $U_i^{j+1}\le\mathbb{W}_i^{j+1}, i=0(1)N$.*

Proof. The matrix $\Phi_{\varepsilon,\mu}^{N,M}U_i^{j+1}$ has a size of $(N+1)\times(N+1)$ with its entries for $i=1(1)N-1$ which are $\mathfrak{Y}^-<0, \mathfrak{Y}^c>0$, and $\mathfrak{Y}^+<0$. As a result, the coefficient matrix meets the M-matrix criteria, ensuring the existence of a positive inverse matrix. This confirms both the existence and uniqueness of the discrete solution. □

Lemma 4.2. *At $(j+1)$th time level, the solution U_i^{j+1} of Eq. (1.1) fulfills the estimate provided below and is bounded.*

$$\left\|U_i^{j+1}\right\| \le \frac{\left\|\Phi_{\varepsilon,\mu}^{N,M}U_i^{j+1}\right\|}{\mathfrak{K}} + \max\left\{\left|\vartheta(t_{j+1})\right|, \left|\xi(t_{j+1})\right|\right\}, \tag{4.1}$$

where $\mathfrak{K} = \min\left\{\frac{\alpha_1}{\varphi}, \frac{\alpha_2}{1-\varphi}\right\}$.

Proof. Let $\mathbb{D} = \dfrac{\left\|\Phi_{\varepsilon,\mu}^{N,M}U_i^{j+1}\right\|}{\mathfrak{K}} + \max\left\{\left|\vartheta(t_{j+1})\right|, \left|\xi(t_{j+1})\right|\right\}$ and define barrier function as

$$\left(\mathfrak{Y}^\pm\right)_i^{j+1} = \mathbb{D} \pm U_i^{j+1}. \tag{4.2}$$

The discrete function $(\mathfrak{Y}\pm)_i^{j+1}$ on the boundaries:

$$\begin{aligned} \mathfrak{Y}^\pm(0,t_{j+1}) &= \mathbb{D}\pm\vartheta(t_{j+1}) = \frac{\left\|\Phi_{\varepsilon,\mu}^{N,M}U_i^{j+1}\right\|}{\mathfrak{K}} + \max\left\{\left|\vartheta(t_{j+1})\right|, \left|\xi(t_{j+1})\right|\right\}\pm\vartheta(t_{j+1})\ge 0, \\ \mathfrak{Y}^\pm(1,t_{j+1}) &= \mathbb{D}\pm\xi(t_{j+1}) = \frac{\left\|\Phi_{\varepsilon,\mu}^{N,M}U_i^{j+1}\right\|}{\mathfrak{K}} + \max\left\{\left|\vartheta(t_{j+1})\right|, \left|\xi(t_{j+1})\right|\right\}\pm\xi(t_{j+1})\ge 0, \end{aligned} \tag{4.3}$$

and on the discretized domain, we have

$$\begin{aligned}\Phi_{\varepsilon,\mu}^{N,M}\left(\mathfrak{Y}^{\pm}\right)_i^{j+1} = \mathbb{D} \pm U_i^{j+1} &= \mathfrak{Y}^{-}\left(\mathbb{D} \pm U_{i-1}^{j+1}\right) + \mathfrak{Y}^{c}\left(\mathbb{D} \pm U_i^{j+1}\right) + \mathfrak{Y}^{+}\left(\mathbb{D} \pm U_{i+1}^{j+1}\right), \\ &= \left(\mathfrak{Y}^{-} + \mathfrak{Y}^{c} + \mathfrak{Y}^{+}\right)\mathbb{D} \pm \mathcal{H}_i^j, \\ &= 2\beta\left(\lambda_1 + \lambda_2\right)\mathbb{D} \pm \mathcal{H}_i^j \geq 0,\end{aligned} \tag{4.4}$$

where $\beta = \max\left(b_l^{j+1} + \frac{c_l^{j+1}}{k}\right)$ for $l = i, i \pm 1$. Lemma 4.1 provides an immediate proof. Consequently, the method maintains uniform stability in the maximum norm. □

Consistent convergence of the discrete scheme in Eq. (3.16) with respect to the parameter can be evaluated by examining the $\mathcal{LTE}$.

Lemma 4.3. *The discrete solution adheres to the subsequent error bound:*

$$\left\|U^{j+1}(x_i) - U_i^{j+1}\right\| \leq Ch^2. \tag{4.5}$$

Proof. The $\mathcal{LTE}$ in space discretization is given as:

$$\begin{aligned}\mathcal{LTE} = \delta(\rho)\varepsilon\left[\frac{U_{i-1}^{j+1} - 2U_i^{j+1} + U_{i+1}^{j+1}}{h^2} - (U_{xx})_i^{j+1}\right] + a_{i-1}^{j+1}\lambda_1\left[\frac{-3U_{i-1}^{j+1} + 4U_i^{j+1} - U_{i+1}^{j+1}}{2h} - (U_x)_{i-1}^{j+1}\right] \\ + 2a_i^{j+1}\lambda_2\left[\frac{U_{i+1}^{j+1} - U_{i-1}^{j+1}}{2h} - (U_x)_i^{j+1}\right] + a_{i+1}^{j+1}\lambda_1\left[\frac{U_{i-1}^{j+1} - 4U_i^{j+1} + 3U_{i+1}^{j+1}}{2h} - (U_x)_{i+1}^{j+1}\right],\end{aligned} \tag{4.6}$$

Using Taylor's expansion of the terms U_{i+1}^{j+1} and U_{i-1}^{j+1}, we have:

$$U_{i\pm1}^{j+1} = U_i^{j+1} \pm h\left(U_x\right)_i^{j+1} + \frac{h^2}{2!}\left(U_{xx}\right)_i^{j+1} \pm \frac{h^3}{3!}\left(U_{xxx}\right)_i^{j+1} + \frac{h^4}{4!}\left(U_{xxxx}\right)_i^{j+1} + \cdots. \tag{4.7}$$

With Eq. (4.7) substituted into Eq. (4.6), we now have

$$\mathcal{LTE} \leq \max_{x_{i-1}\leq x\leq x_{i+1}}\left[\frac{\delta(\rho)_i\varepsilon h^2}{12}\left|\left(U_{xxxx}\right)_i^{j+1}\right|\right] + \max_{x_{i-1}\leq x\leq x_{i+1}}\left[\frac{\lambda_2 a_i^{j+1}h^2}{3}\left|\left(U_{xxx}\right)_i^{j+1}\right|\right]. \tag{4.8}$$

Using $\mathcal{J} = \rho\mu(\lambda_1 + \lambda_2)a^{j+1}(i)\coth\left(\frac{\rho\mu a^{j+1}(i)}{2}\right)$ in Eq. (4.8) where $\rho = h/\varepsilon$, we have:

$$\begin{aligned}|\mathcal{LTE}| &\leq \max_{x_{i-1}\leq x\leq x_{i+1}}\left[\mathcal{J}h^3 12\left|\left(U_{xxxx}\right)_i^{j+1}\right|\right] + \max_{x_{i-1}\leq x\leq x_{i+1}}\left[\frac{\lambda_2 a_i^{j+1}h^2}{3}\left|\left(U_{xxx}\right)_i^{j+1}\right|\right], \\ &\leq \max_{x_{i-1}\leq x\leq x_{i+1}}\left[\frac{\lambda_2 a_i^{j+1}h^2}{3}\left|\left(U_{xxx}\right)_i^{j+1}\right|\right] + O(h^3) \leq O(h^2), \quad i = 1(1)N-1.\end{aligned} \tag{4.9}$$

As a result, the stability estimate of scheme is implied, and boundedness of $\mathcal{LTE}$ in space discretization is guaranteed. Now, Eq. (3.16) can be written as:

$$\left[-\frac{\delta(\rho)\varepsilon}{h^2} + \bar{w}_i\right]U_{i-1}^{j+1} + \left[2\frac{\delta(\rho)\varepsilon}{h^2} + \bar{f}_i\right]U_i^{j+1} + \left[-\frac{\delta(\rho)\varepsilon}{h^2} + \bar{c}_i\right]U_{i+1}^{j+1} + \mathfrak{X}_i + \mathcal{LTE}_i = 0, \tag{4.10}$$

where

$$\begin{cases} \bar{w}_i = \dfrac{3\lambda_1}{2h}\mu a_{i-1}^{j+1} + \dfrac{\lambda_2}{h}\mu a_i^{j+1} - \dfrac{\lambda_1}{2h}\mu a_{i+1}^{j+1} + \lambda_1\left(b_{i-1}^{j+1} + \frac{c_{i-1}^{j+1}}{k}\right), \\ \bar{f}_i = -\dfrac{2\lambda_1}{h}\mu a_{i-1}^{j+1} + \dfrac{2\lambda_1}{h}\mu a_{i+1}^{j+1} + 2\lambda_2\left(b_i^{j+1} + \frac{c_i^{j+1}}{k}\right), \\ \bar{c}_i = \dfrac{\lambda_1}{2h}\mu a_{i-1}^{j+1} - \dfrac{\lambda_2}{h}\mu a_i^{j+1} - \dfrac{3\lambda_1}{2h}\mu a_{i+1}^{j+1} + \lambda_1\left(b_{i+1}^{j+1} + \frac{c_{i+1}^{j+1}}{k}\right), \\ \mathfrak{X}_i = \lambda_1\left[\varpi_{i-1}^{j+1} - \frac{c_{i-1}^{j}}{k}U_{i-1}^{j}\right] + 2\lambda_2\left[\varpi_{i-1}^{j+1} - \frac{c_i^{j}}{k}U_i^{j}\right] + \lambda_1\left[\varpi_{i+1}^{j+1} - \frac{c_{i+1}^{j}}{k}U_{i+1}^{j}\right]. \end{cases} \tag{4.11}$$

By imposing boundary conditions on Eq. (4.10), we can write in matrix form as:

$$[\mathbb{S}+\mathbb{I}]\,U + \mathcal{K} + \mathcal{L}\mathcal{T}\mathcal{E}_i = 0, \tag{4.12}$$

where $\mathbb{S} = trid\left[-\dfrac{\delta(\rho)\varepsilon}{h^2}, 2\dfrac{\delta(\rho)\varepsilon}{h^2}, -\dfrac{\delta(\rho)\varepsilon}{h^2}\right], \mathbb{I} = trid\left[\bar{w}_i, \bar{f}_i, \bar{c}_i\right]$ are $(N-1)\times(N-1)$ tridiagonal matrices, $\mathcal{K} = \left[\mathfrak{X}_1 + \left[-\dfrac{\delta(\rho)\varepsilon}{h^2} + \bar{w}_1\right]\vartheta_0^{j+1}, \mathfrak{X}_2, ..., \mathfrak{X}_{N-2}, \mathfrak{X}_{N-1} + \left[-\dfrac{\delta(\rho)\varepsilon}{h^2} + \bar{c}_{N-1}\right]\xi_N^{j+1}\right]$, and $U = \left[U_1^{j+1}, ..., U_{N-1}^{j+1}\right]^T$, are component vectors of Eq. (4.12). Let $\bar{\mathfrak{U}} = \left[\bar{\mathfrak{U}}_1^{j+1}, \bar{\mathfrak{U}}_2^{j+1}, ..., \bar{\mathfrak{U}}_{N-1}^{j+1}\right] \cong U$ satisfy the following expression:

$$[\mathbb{S}+\mathbb{I}]\,\bar{\mathfrak{U}} + \mathcal{K} = 0. \tag{4.13}$$

Subtracting Eq. (4.12) from Eq. (4.13), we obtain:

$$[\mathbb{S}+\mathbb{I}]\,\mathbb{E} = \mathcal{L}\mathcal{T}\mathcal{E}_i, \tag{4.14}$$

where $\mathbb{E} = \bar{\mathfrak{U}} - U = [\grave{e}_1, \grave{e}_2, ..., \grave{e}_{N-1}]^T$ is the discretization error. Let $\left|a_s^{j+1}\right| \le \mathcal{C}_1$, $\left|b_s^{j+1}\right| \le \mathcal{C}_2$ and $\left|c_s^{j+1}\right| \le \mathcal{C}_3$, $s = i, i\pm1$, where $\mathcal{C}_1, \mathcal{C}_2, \mathcal{C}_3$ are positive constants. Multiplying Eq. (4.10) by h and let $\ddot{r}_{ij}$ be the $(i,j)th$ element of the matrix $\mathbb{I}$; then for $i = 1(1)N-1$:

$$\begin{aligned} |\mathbb{I}_{i,i+1}| = |\bar{c}_i| &\le -\mu\mathcal{C}_1(\lambda_1+\lambda_1) + h\lambda_1\left(\mathcal{C}_2 + \frac{\mathcal{C}_3}{k}\right), \quad i = 1(1)N-2, \\ |\mathbb{I}_{i,i-1}| = |\bar{w}_i| &\le \mu\mathcal{C}_1(\lambda_1+\lambda_1) + h\lambda_1\left(\mathcal{C}_2 + \frac{\mathcal{C}_3}{k}\right), \quad i = 2(1)N-1. \end{aligned} \tag{4.15}$$

Thus, for adequately small h, i.e., as $h \to 0$, we obtain:

$$\begin{cases} -\dfrac{\delta(\rho)}{\rho} + |\mathbb{I}_{i,i+1}| \ne 0, \quad i = 1(1)N-2, \\ -\dfrac{\delta(\rho)}{\rho} + |\mathbb{I}_{i,i-1}| \ne 0, \quad i = 2(1)N-1, \quad \rho = h/\varepsilon. \end{cases} \tag{4.16}$$

Let the matrix $(\mathbb{S}+\mathbb{I})$ has $\mathfrak{L}_i$ as the sum of its $i-$th row elements, we get:

$$\begin{aligned} \mathfrak{L}_1 &= \sum_{m=1}^{N-1}\mathbb{R}_{1,j} = \frac{\delta(\rho)}{\rho} - \frac{3\lambda_1}{2}\mu a_{i-1}^{j+1} - \lambda_2\mu a_i^{j+1} + \frac{\lambda_1}{2}\mu a_{i+1}^{j+1} + h\left(2\lambda_2\beta_i^{j+1} + \lambda_1\beta_{i+1}^{j+1}\right), i = 1, \\ \mathfrak{L}_i &= \sum_{m=2}^{N-2}\mathbb{R}_{i,j} = h\left(\lambda_1\beta_{i-1}^{j+1} + 2\lambda_2\beta_i^{j+1} + \lambda_2\beta_{i+1}^{j+1}\right) + O(h^2) = \beta_i^{j+1} + O(h^2), i = 2(1)N-2, \\ \mathfrak{L}_{N-1} &= \sum_{m=1}^{N-1}\mathbb{R}_{N-1,j} = \frac{\delta(\rho)}{\rho} - \frac{\lambda_1}{2}\mu a_{i-1}^{j+1} + \lambda_2\mu a_i^{j+1} + \frac{3\lambda_1}{2}\mu a_{i+1}^{j+1} + h\left(\lambda_1\beta_{i-1}^{j+1} + 2\lambda_2\beta_i^{j+1}\right), i = N-1, \end{aligned} \tag{4.17}$$

where $\beta_i^{j+1} = \left(b_i^{j+1} + c_i^{j+1}/k\right)$. The matrix $(\mathbb{S}+\mathbb{I})$ is irreducible if the matrix satisfies Eq. (4.16) [9, 22, 23]. The matrix $(\mathbb{S}+\mathbb{I})$ is monotone for sufficiently small h. Hence, $(\mathbb{S}+\mathbb{I})^{-1}$ exist and $(\mathbb{S}+\mathbb{I})^{-1} \ge 0$. We obtain from Eq. (4.14)

that:

$$\mathbb{E} = [\mathbb{S} + \mathbb{I}]^{-1} \mathcal{LTE}_i. \tag{4.18}$$

Eq. (4.18) can be expressed as follows by using the matrix norm

$$\|\mathbb{E}\| \leq \left\|[\mathbb{S} + \mathbb{I}]^{-1}\right\| \mathcal{LTE}. \tag{4.19}$$

Assume that the (m,n)th elements of $(\mathbb{S}+\mathbb{I})^{-1}$ are $\hat{r}_{m,n}$, and we define $\left\|(\hat{r})^{-1}_{m,n}\right\| = \max_{1\leq m\leq N-1} \sum_{n=1}^{N-1} \left|(\hat{r})^{-1}_{m,n}\right|$. Given that $(\hat{r})^{-1}_{m,n} \geq 0$, we can derive:

$$\sum_{n=1}^{N-1} \hat{r}_{m,n}\mathfrak{L}_i = 1 \Rightarrow \sum_{n=1}^{N-1} \hat{r}_{m,n} \leq \frac{1}{\min_{0\leq n\leq N-1} \mathfrak{L}_i} \leq \frac{1}{\left|\beta_i^{j+1}\right|}, \quad m = 1(1)N-1. \tag{4.20}$$

Thus, from Eqs. (4.10), (4.19), (4.20), and (4.9), we obtain:

$$\mathbb{E}_i = \sum_{n=1}^{N-1} \hat{r}_{m,n}\mathcal{LTE}_i \leq \frac{O(h^2)}{\left|\beta_i^{j+1}\right|}, \quad m = 1(1)N-1. \tag{4.21}$$

For this reason, $\|\mathbb{E}\| \leq O(h^2)$, indicating that the method exhibits second-order convergence in the spatial direction during the semi-discretization process. □

Theorem 4.4. *Let $u(x,t)$ and U_i^{j+1} are solution of Eq. (1.1) and approximate solution Eq. (3.16), respectively. Next, we have the fully discrete scheme error estimate which is given by*

$$\max_{0<\varepsilon,\mu\leq 1} \left\|u(x_i,t_{j+1}) - U_i^{j+1}\right\|_\infty \leq C\left(k + h^2\right). \tag{4.22}$$

Proof. The desired estimate, possessing first-order accuracy in time and second-order accuracy in space, is obtained by combining Lemma 3.2 with Lemma 4.3. □

5. Example Problems and Numerical Findings

We perform several tests using the recommended numerical method to solve various examples, thereby supporting the proposed theory. We determine the maximum pointwise error and convergence rate using the double mesh method [23]. Maximum error $(\tilde{E}^{N,M}_{\varepsilon,\mu})$ is given as:

$$\tilde{E}^{N,M}_{\varepsilon,\mu} = \max_{0\leq i,j\leq N,M} \left|U^{N,M}_{i,j} - U^{2N,2M}_{i,j}\right|. \tag{5.1}$$

Here, $U^{N,M}_{i,j}$ represents the numerical solutions obtained employing the suggested method on a uniform mesh. To compute $U^{2N,2M}_{i,j}$, additionl intervals are introduced by doubling N and M and selecting the midpoints of all previously defined intervals in both spatial and temporal directions [8, 15]. Rate of convergence$(\mathfrak{R}^{N,M}_{\varepsilon,\mu})$ is given as:

$$\mathfrak{R}^{N,M}_{\varepsilon,\mu} = \frac{\log\left(\tilde{E}^{N,M}_{\varepsilon,\mu}/\tilde{E}^{2N,2M}_{\varepsilon,\mu}\right)}{\log(2)}. \tag{5.2}$$

We examine four distinct cases to demonstrate the characteristics of layer phenomena for all possible signs variation between $a(x,t)$ and $\varpi(x,t)$.

Example 5.1. In this problem, we take $\Omega = (0,1)$ and $\varphi = 0.5$ [3, 21].

$$\begin{cases} \varepsilon\dfrac{\partial^2 u}{\partial x^2} + \mu a(x,t)\dfrac{\partial u}{\partial x} - (1+e^x)u - \dfrac{\partial u}{\partial t} = \varpi(x,t), (x,t) \in \mathfrak{Q}^- \cup \mathfrak{Q}^+, \\ u(0,t) = 0 \quad \text{on} \quad \mathfrak{Q}_l, \quad u(1,t) = 0 \quad \text{on} \quad \mathfrak{Q}_r, \\ u(x,0) = 0 \quad \text{on} \quad \mathfrak{Q}_b, \end{cases} \tag{5.3}$$

where $a(x,t)=\begin{cases}-\left(1+x-x^2\right), & (x,t)\in\mathfrak{Q}^-,\\ \left(1+x-x^2\right), & (x,t)\in\mathfrak{Q}^-,\end{cases}$ $\varpi(x,t)=\begin{cases}-2t\left(1+x^2\right), & (x,t)\in\mathfrak{Q}^-,\\ 2t\left(1+x^2\right), & (x,t)\in\mathfrak{Q}^-.\end{cases}$

Example 5.2. Consider the second test problem with non-smooth data [2].

$$\begin{cases}\varepsilon\dfrac{\partial^2 u}{\partial x^2}+\mu a(x,t)\dfrac{\partial u}{\partial x}-(1+e^x)u-\dfrac{\partial u}{\partial t}=\varpi(x,t),(x,t)\in\mathfrak{Q}^-\cup\mathfrak{Q}^+,\\ u(0,t)=0 \quad \text{on} \quad \mathfrak{Q}_l, \quad u(1,t)=0 \quad \text{on} \quad \mathfrak{Q}_r,\\ u(x,0)=0 \quad \text{on} \quad \mathfrak{Q}_b,\end{cases} \tag{5.4}$$

where $a(x,t)=\begin{cases}(x+2), & 0\le x\le 0.5,\\ -(2x+3), & 0.5<x\le 1,\end{cases}$ $\varpi(x,t)=\begin{cases}t(2x+1), & 0\le x\le 0.5,\\ -t(3x+4), & 0.5<x\le 1.\end{cases}$

Example 5.3. Let us take Eq. (1.1) and its coefficients to be [2]

$a(x,t)=\begin{cases}-(1+e^{-xt}), & 0\le x\le 0.5,\\ (2+x+t), & 0.5<x\le 1,\end{cases}$ $\varpi(x,t)=\begin{cases}\left(e^{t^2}-1\right)(1+xt), & 0\le x\le 0.5,\\ -t^2(2+x), & 0.5<x\le 1,\end{cases}$

$b(x,t)=2+xt, c(,t)=1, \quad u(0,t)=0=u(1,t)$, and $u(x,0)=0$.

Example 5.4. Let us take Eq. (1.1) and its coefficients to be [2]

$a(x,t)=\begin{cases}\left(1+x-x^2+t\right), & (x,t)\in\mathfrak{Q}^-,\\ -(1+3xt), & (x,t)\in\mathfrak{Q}^+,\end{cases}$ $\varpi(x,t)=\begin{cases}(e^t-1)(1+x), & (x,t)\in\mathfrak{Q}^-,\\ t(x-2), & (x,t)\in\mathfrak{Q}^+,\end{cases}$

$b(x,t)=1+x+t, c(x,t)=1, \quad u(0,t)=0=u(1,t)$, and $u(x,0)=0$.

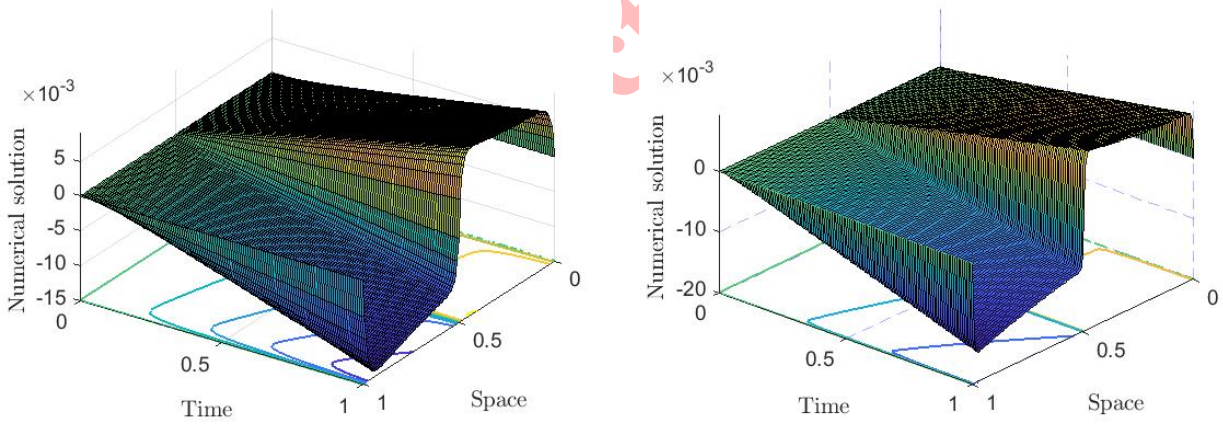

(a) $\varepsilon=2^{-4},\mu=1$ (b) $\varepsilon=2^{-12},\mu=2^{-12}$

FIGURE 2. The numerical solution profile for Example 5.1.

The $\tilde{E}^{N,M}_{\varepsilon,\mu}$ and $\mathfrak{R}^{N,M}_{\varepsilon,\mu}$ for Examples 5.1–5.4 are displayed in Tables 1–4 using various values of ε,μ. Notably, in every example, there is an abrupt change in neighborhood of $x=0.5$ due to discontinuity in convection coefficients and source terms. In Tables 1 and 4, we analyze a constant μ while adjusting ε, demonstrating results that exhibit nearly first-order uniform convergence. We take a fixed value of ε and vary μ to present almost first- order uniform convergent results in Tables 2 and 3. These four tables' numerical results support our theoretical assertions that the suggested scheme yields uniform outcomes in both scenarios. The tables show that, in both cases, for fixed N,M, the maximum point-wise error is constant at a given small ε or μ. This demonstrates that the approach is independent

TABLE 1. Computed $\tilde{E}^{N,M}_{\varepsilon,\mu}$ and $\mathfrak{R}^{N,M}_{\varepsilon,\mu}$ when $\mu = 2^{-4}$ for Example 5.1.

Mesh points count: N equals M						
$\varepsilon \downarrow$	16	32	64	128	256	512
2^{0}	$1.9460e-02$	$1.4727e-02$	$9.8114e-03$	$5.7649e-03$	$3.1369e-03$	$1.6573e-03$
	$4.0205e-01$	$5.8593e-01$	$7.6716e-01$	$8.7796e-01$	$9.2050e-01$	–
2^{-2}	$3.7203e-02$	$2.2243e-02$	$1.2298e-02$	$6.5594e-03$	$3.4347e-03$	$1.7763e-03$
	$7.4207e-01$	$8.5493e-01$	$9.0679e-01$	$9.3338e-01$	$9.5131e-01$	–
2^{-4}	$4.4987e-02$	$2.5013e-02$	$1.3410e-02$	$7.0215e-03$	$3.6197e-03$	$1.8487e-03$
	$8.4683e-01$	$8.9937e-01$	$9.3346e-01$	$9.5591e-01$	$9.6936e-01$	–
2^{-6}	$4.8237e-02$	$2.6584e-02$	$1.4097e-02$	$7.2966e-03$	$3.7278e-03$	$1.8907e-03$
	$8.5958e-01$	$9.1517e-01$	$9.5009e-01$	$9.6890e-01$	$9.7940e-01$	–
2^{-8}	$4.9256e-02$	$2.7424e-02$	$1.4433e-02$	$7.4428e-03$	$3.7896e-03$	$1.9143e-03$
	$8.4486e-01$	$9.2607e-01$	$9.5545e-01$	$9.7380e-01$	$9.8523e-01$	–
2^{-10}	$4.9365e-02$	$2.7629e-02$	$1.4632e-02$	$7.5114e-03$	$3.8199e-03$	$1.9262e-03$
	$8.3731e-01$	$9.1706e-01$	$9.6197e-01$	$9.7555e-01$	$9.8778e-01$	–
2^{-12}	$4.9368e-02$	$2.7644e-02$	$1.4667e-02$	$7.5563e-03$	$3.8304e-03$	$1.9329e-03$
	$8.3661e-01$	$9.1439e-01$	$9.5682e-01$	$9.8018e-01$	$9.8673e-01$	–
2^{-14}	$4.9368e-02$	$2.7644e-02$	$1.4668e-02$	$7.5606e-03$	$3.8387e-03$	$1.9341e-03$
	$8.3661e-01$	$9.1439e-01$	$9.5682e-01$	$9.8018e-01$	$9.8896e-01$	–
2^{-16}	$4.9368e-02$	$2.7644e-02$	$1.4668e-02$	$7.5606e-03$	$3.8390e-03$	$1.9344e-03$
	$8.3661e-01$	$9.1439e-01$	$9.5682e-01$	$9.8018e-01$	$9.8884e-01$	–
⋮	⋮	⋮	⋮	⋮	⋮	⋮
2^{-30}	$4.9368e-02$	$2.7644e-02$	$1.4668e-02$	$7.5606e-03$	$3.8390e-03$	$1.9344e-03$
	$8.3661e-01$	$9.1439e-01$	$9.5682e-01$	$9.8018e-01$	$9.8884e-01$	–
$\tilde{E}^{N,M}_{\varepsilon,\mu}$	$4.9368e-02$	$2.7644e-02$	$1.4668e-02$	$7.5606e-03$	$3.8390e-03$	$1.9344e-03$
$\mathfrak{R}^{N,M}_{\varepsilon,\mu}$	$8.3661e-01$	$9.1439e-01$	$9.5682e-01$	$9.8018e-01$	$9.8884e-01$	–

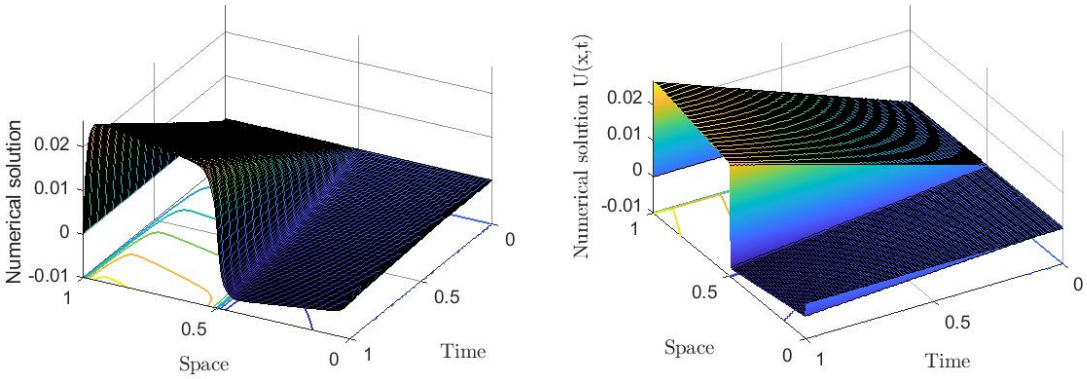

(a) $\varepsilon = 2^{-4}, \mu = 2^{-2}$. (b) $\varepsilon = 2^{-12}, \mu = 2^{-18}$.

FIGURE 3. The numerical solution profile for Example 5.2.

of ε and μ. Table 5 compare numerical results to those given in [2, 3], by fixing or varying ε or μ. This comparison reveals that, when evaluated against existing studies in the literature, the proposed approach yields a more precise solution. Every result shown in the tables was acquired by taking $N = M$.

TABLE 2. Computed $\tilde{E}^{N,M}_{\varepsilon,\mu}$ and $\mathfrak{R}^{N,M}_{\varepsilon,\mu}$ for $\varepsilon = 2^{-12}$ for Example 5.2.

For equal values of mesh points:$N = M$						
$\mu \downarrow$	16	32	64	128	256	512
2^{0}	$8.1573e-02$	$4.8402e-02$	$2.5717e-02$	$1.3251e-02$	$6.7289e-03$	$3.3910e-03$
	$7.5303e-01$	$9.1234e-01$	$9.5662e-01$	$9.7766e-01$	$9.8866e-01$	–
2^{-2}	$9.2766e-02$	$5.0196e-02$	$2.6171e-02$	$1.3372e-02$	$6.7601e-03$	$3.3988e-03$
	$8.8602e-01$	$9.3960e-01$	$9.6875e-01$	$9.8410e-01$	$9.9202e-01$	–
2^{-4}	$9.4033e-02$	$5.0576e-02$	$2.6278e-02$	$1.3400e-02$	$6.7563e-03$	$3.3970e-03$
	$8.9471e-01$	$9.4460e-01$	$9.7162e-01$	$9.8793e-01$	$9.9197e-01$	–
2^{-6}	$9.4376e-02$	$5.0684e-02$	$2.6295e-02$	$1.3365e-02$	$6.7555e-03$	$3.3952e-03$
	$8.9689e-01$	$9.4674e-01$	$9.7633e-01$	$9.8433e-01$	$9.9257e-01$	–
2^{-8}	$9.4453e-02$	$5.0624e-02$	$2.6150e-02$	$1.3364e-02$	$6.7506e-03$	$3.3949e-03$
	$8.9978e-01$	$9.5301e-01$	$9.6846e-01$	$9.8526e-01$	$9.9165e-01$	–
2^{-10}	$9.4309e-02$	$5.0443e-02$	$2.6151e-02$	$1.3363e-02$	$6.7486e-03$	$3.3948e-03$
	$9.0274e-01$	$9.4779e-01$	$9.6862e-01$	$9.8558e-01$	$9.9126e-01$	–
2^{-12}	$9.4194e-02$	$5.0368e-02$	$2.6151e-02$	$1.3363e-02$	$6.7480e-03$	$3.3947e-03$
	$9.0313e-01$	$9.4564e-01$	$9.6862e-01$	$9.8571e-01$	$9.9118e-01$	–
2^{-14}	$9.4158e-02$	$5.0347e-02$	$2.6151e-02$	$1.3362e-02$	$6.7478e-03$	$3.3947e-03$
	$9.0318e-01$	$9.4504e-01$	$9.6873e-01$	$9.8565e-01$	$9.9113e-01$	–
2^{-16}	$9.4148e-02$	$5.0342e-02$	$2.6151e-02$	$1.3362e-02$	$6.7478e-03$	$3.3947e-03$
	$9.0317e-01$	$9.4490e-01$	$9.6873e-01$	$9.8565e-01$	$9.9113e-01$	–
2^{-18}	$9.4145e-02$	$5.0340e-02$	$2.6151e-02$	$1.3362e-02$	$6.7478e-03$	$3.3947e-03$
	$9.0319e-01$	$9.4484e-01$	$9.6873e-01$	$9.8565e-01$	$9.9113e-01$	–
$\vdots$		$\vdots$		$\vdots$		$\vdots$
2^{-24}	$9.4145e-02$	$5.0340e-02$	$2.6151e-02$	$1.3362e-02$	$6.7478e-03$	$3.3947e-03$
	$9.0318e-01$	$9.4484e-01$	$9.6873e-01$	$9.8565e-01$	$9.9113e-01$	–
$\tilde{E}^{N,M}_{\varepsilon,\mu}$	$9.4453e-02$	$5.0684e-02$	$2.6295e-02$	$1.3400e-02$	$6.7601e-03$	$3.3988e-03$
$\mathfrak{R}^{N,M}_{\varepsilon,\mu}$	$8.9807e-01$	$9.4674e-01$	$9.7256e-01$	$9.8712e-01$	$9.9202e-01$	–

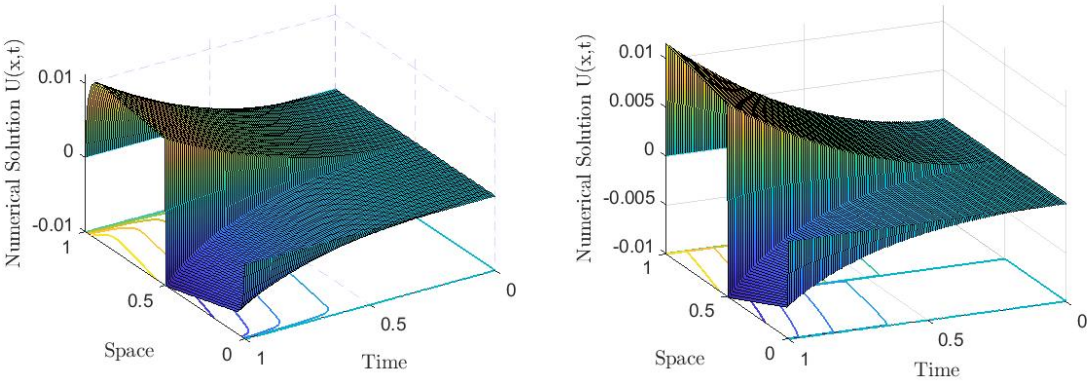

(a) $\varepsilon = 2^{-8}, \mu = 1$. (b) $\varepsilon = 2^{-12}, \mu = 2^{-8}$.

FIGURE 4. Surface-contour plots for Example 5.3.

The solution profiles in the form of surface-contour plots are provided in Figures 2, 3, 4, and 5 for Examples 5.1, 5.2, 5.3, and 5.4 respectively to illustrate how the gradient of solution steepens at the point of discontinuity when ε

TABLE 3. Computed $\tilde{E}^{N,M}_{\varepsilon,\mu}$ and $\mathfrak{R}^{N,M}_{\varepsilon,\mu}$ with $\varepsilon = 2^{-8}$ for Example 5.3.

$N = M$						
$\mu \downarrow$	16	32	64	128	256	512
2^{0}	$3.7484e-02$	$2.0606e-02$	$1.0889e-02$	$5.6228e-03$	$2.8631e-03$	$1.4459e-03$
	$8.6321e-01$	$9.2019e-01$	$9.5351e-01$	$9.7371e-01$	$9.8561e-01$	–
2^{-2}	$4.0906e-02$	$2.1744e-02$	$1.1240e-02$	$5.7237e-03$	$2.8898e-03$	$1.4522e-03$
	$9.1170e-01$	$9.5198e-01$	$9.7362e-01$	$9.8598e-01$	$9.9273e-01$	–
2^{-4}	$4.2102e-02$	$2.2153e-02$	$1.1342e-02$	$5.7474e-03$	$2.8948e-03$	$1.4535e-03$
	$9.2639e-01$	$9.6583e-01$	$9.8069e-01$	$9.8945e-01$	$9.9393e-01$	–
2^{-6}	$4.2736e-02$	$2.2209e-02$	$1.1373e-02$	$5.7531e-03$	$2.8960e-03$	$1.4537e-03$
	$9.4431e-01$	$9.6553e-01$	$9.8320e-01$	$9.9028e-01$	$9.9433e-01$	–
2^{-8}	$4.2794e-02$	$2.2266e-02$	$1.1378e-02$	$5.7547e-03$	$2.8962e-03$	$1.4538e-03$
	$9.4257e-01$	$9.6860e-01$	$9.8343e-01$	$9.9058e-01$	$9.9433e-01$	–
2^{-10}	$4.2802e-02$	$2.2277e-02$	$1.1380e-02$	$5.7550e-03$	$2.8963e-03$	$1.4538e-03$
	$9.4212e-011$	$9.6905e-01$	$9.8361e-01$	$9.9060e-01$	$9.9438e-01$	–
2^{-12}	$4.2804e-02$	$2.2280e-02$	$1.1380e-02$	$5.7551e-03$	$2.8963e-03$	$1.4538e-03$
	$9.4200e-01$	$9.6925e-01$	$9.8359e-01$	$9.9063e-01$	$9.9438e-01$	–
2^{-14}	$4.2804e-02$	$2.2281e-02$	$1.1380e-02$	$5.7551e-03$	$2.8963e-03$	$1.4538e-03$
	$9.4193e-01$	$9.6931e-01$	$9.8359e-01$	$9.9063e-01$	$9.9438e-01$	–
⋮	⋮			⋮		⋮
2^{-24}	$4.2804e-02$	$2.2281e-02$	$1.1380e-02$	$5.7551e-03$	$2.8963e-03$	$1.4538e-03$
	$9.4193e-01$	$9.6931e-01$	$9.8359e-01$	$9.9063e-01$	$9.9438e-01$	–
$\tilde{E}^{N,M}_{\varepsilon,\mu}$	$4.2804e-02$	$2.2281e-02$	$1.1380e-02$	$5.7551e-03$	$2.8963e-03$	$1.4538e-03$
$\mathfrak{R}^{N,M}_{\varepsilon,\mu}$	$9.4193e-01$	$9.6931e-01$	$9.8359e-01$	$9.9063e-01$	$9.9438e-01$	–

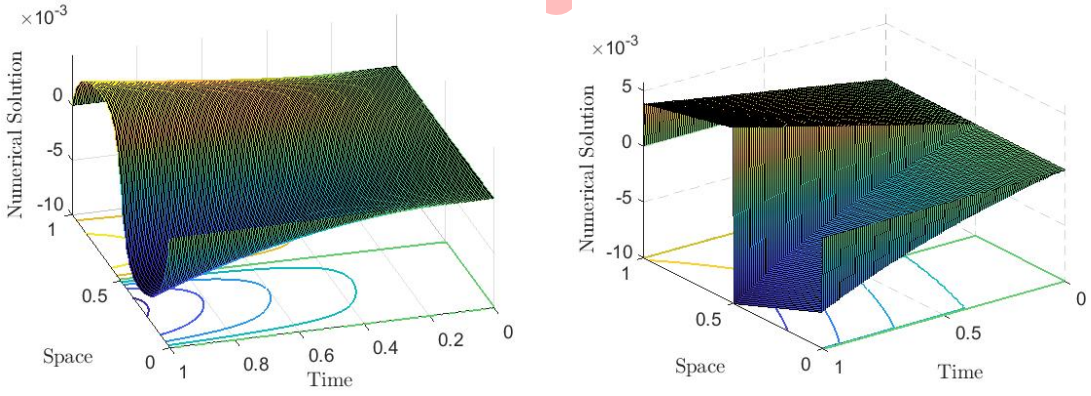

(a) $\varepsilon = 1, \mu = 2^{-6}$. (b) $\varepsilon = 2^{-16}, \mu = 2^{-16}$.

FIGURE 5. Surface plots for Example 5.4.

or μ decreases. Due to the occurrence of ε, μ and discontinuous data in the convection and source terms, the surface plots of the numerical solution show the presence of layers(both boundary and interior). We notice a decrement in the layer width as we decrease μ or ε (see Figures 2(a), 3(a), 4(a), and 5(a)). The line plots for Examples 5.1, 5.2, 5.3, and 5.4 at various time steps while maintaining $N = 128 = M$ are represented in Figures 7, 8, 9, and 10, which show that the maximum error occurs near the boundary and interior layer regions. The observation of a sharper layer as

TABLE 4. Computed $\tilde{E}^{N,M}_{\varepsilon,\mu}$ and $\mathfrak{R}^{N,M}_{\varepsilon,\mu}$ for $\mu = 2^{-10}$ and various values of ε for Example 5.4.

For equal mesh points in both directions						
$\varepsilon \downarrow$	16	32	64	128	256	512
2^{0}	$1.1487e-02$	$1.0042e-02$	$6.8505e-03$	$3.9935e-03$	$2.1448e-03$	$1.1189e-03$
	$1.9396e-01$	$5.5177e-01$	$7.7856e-01$	$8.9681e-01$	$9.3876e-01$	–
2^{-2}	$2.5450e-02$	$1.5559e-02$	$8.4794e-03$	$4.4495e-03$	$2.3003e-03$	$1.1781e-03$
	$7.0992e-01$	$8.7572e-01$	$9.3032e-01$	$9.5182e-01$	$9.6536e-01$	–
2^{-4}	$3.2209e-02$	$1.7363e-02$	$9.0907e-03$	$4.6828e-03$	$2.3901e-03$	$1.2124e-03$
	$8.9145e-01$	$9.3355e-01$	$9.5702e-01$	$9.7030e-01$	$9.7921e-01$	–
2^{-6}	$3.4363e-02$	$1.8239e-02$	$9.4273e-03$	$4.8172e-03$	$2.4416e-03$	$1.2317e-03$
	$9.1383e-01$	$9.5211e-01$	$9.6865e-01$	$9.8037e-01$	$9.8718e-01$	–
2^{-8}	$3.5276e-02$	$1.8709e-02$	$9.6213e-03$	$4.8915e-03$	$2.4692e-03$	$1.2425e-03$
	$9.1495e-01$	$9.5943e-01$	$9.7595e-01$	$9.8623e-01$	$9.9080e-01$	–
2^{-10}	$3.5937e-02$	$1.8866e-02$	$9.7252e-03$	$4.9261e-03$	$2.4834e-03$	$1.2481e-03$
	$9.2968e-01$	$9.5599e-01$	$9.8128e-01$	$9.8813e-01$	$9.9258e-01$	–
2^{-12}	$3.6573e-02$	$1.9011e-02$	$9.7482e-03$	$4.9507e-03$	$2.4904e-03$	$1.2512e-03$
	$9.4394e-01$	$9.6363e-01$	$9.7750e-01$	$9.9126e-01$	$9.9307e-01$	–
2^{-14}	$3.6721e-02$	$1.9177e-02$	$9.7742e-03$	$4.9538e-03$	$2.4966e-03$	$1.2526e-03$
	$9.3723e-01$	$9.7233e-01$	$9.8044e-01$	$9.8857e-01$	$9.9504e-01$	–
2^{-16}	$3.6735e-02$	$1.9207e-02$	$9.8141e-03$	$4.9548e-03$	$2.4970e-03$	$1.2534e-03$
	$9.3552e-01$	$9.6870e-01$	$9.8603e-01$	$9.8863e-01$	$9.9435e-01$	–
2^{-18}	$3.6735e-02$	$1.9208e-02$	$9.8180e-03$	$4.9627e-03$	$2.4969e-03$	$1.2535e-03$
	$9.3545e-01$	$9.6821e-01$	$9.8430e-01$	$9.9099e-01$	$9.9418e-01$	–
⋮		⋮		⋮		⋮
2^{-24}	$3.6735e-02$	$1.9208e-02$	$9.8180e-03$	$4.9629e-03$	$2.4969e-03$	$1.2535e-03$
	$9.3545e-01$	$9.6821e-01$	$9.8425e-01$	$9.9105e-01$	$9.9418e-01$	–
$\tilde{E}^{N,M}_{\varepsilon,\mu}$	$3.6735e-02$	$1.9208e-02$	$9.8180e-03$	$4.9629e-03$	$2.4969e-03$	$1.2535e-03$
$\mathfrak{R}^{N,M}_{\varepsilon,\mu}$	$9.3545e-01$	$9.6821e-01$	$9.8425e-01$	$9.9105e-01$	$9.9418e-01$	–

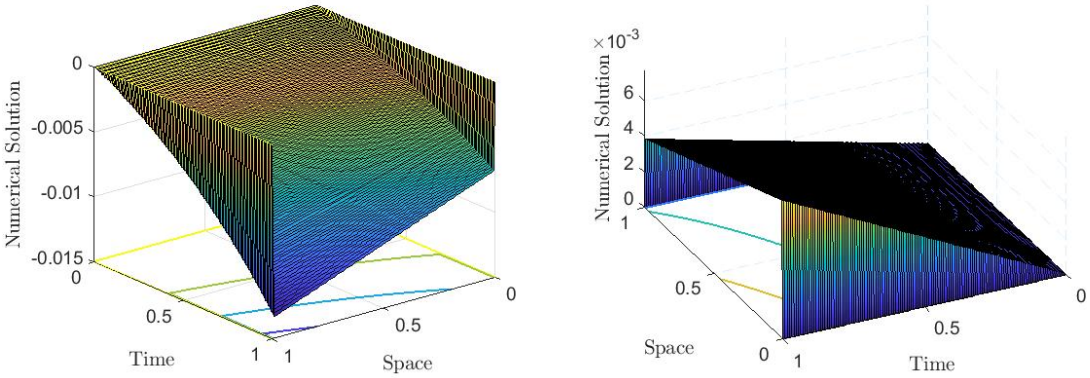

(a) Source term is $\varpi(x,t) = \left(e^{t}-1\right)(1+x)$.

(b) Source term is $\varpi(x,t) = t(x-2)$.

FIGURE 6. Numerical solution for Example 5.4 with $\varepsilon = 2^{-16}$ and $\mu = 2^{-16}$.

we decrease the values of ε and μ is confirmed, which helps us understand the influence of parameter values and how they affect the formation of layers. Every line plots and surface plots are created for fixed values of $N = M = 128$.

TABLE 5. Comparison of $\tilde{E}^{N,M}_{\varepsilon,\mu}$ and $\mathfrak{R}^{N,M}_{\varepsilon,\mu}$ for Example 5.1-5.4.

$(N = M) \rightarrow$	64	128	256	512
Present Method for Example 5.1				
$\tilde{E}^{N,M}_{\varepsilon,\mu}$	$1.4668e-02$	$7.5606e-03$	$3.8390e-03$	$1.9344e-03$
$\mathfrak{R}^{N,M}_{\varepsilon,\mu}$	$9.5682e-01$	$9.8018e-01$	$9.8884e-01$	–
Result in [3](Upwind scheme on piecewise uniform mesh)				
$\tilde{E}^{N,M}_{\varepsilon,\mu}$	$8.2743e-2$	$5.2731e-2$	$3.0348e-2$	$1.647e-2$
$\mathfrak{R}^{N,M}_{\varepsilon,\mu}$	$6.4997e-01$	$7.9705e-01$	$8.8105e-01$	–
Present Method for Example 5.2				
$\tilde{E}^{N,M}_{\varepsilon,\mu}$	$2.6295e-02$	$1.3400e-02$	$6.7601e-03$	$3.3988e-03$
$\mathfrak{R}^{N,M}_{\varepsilon,\mu}$	$9.7256e-01$	$9.8712e-01$	$9.9202e-01$	–
Result in [2](Upwind scheme on piecewise uniform mesh)				
$\tilde{E}^{N,M}_{\varepsilon,\mu}$	$2.3788e-02$	$1.8358e-02$	$1.2613e-02$	$8.0788e-03$
$\mathfrak{R}^{N,M}_{\varepsilon,\mu}$	$3.7381e-01$	$5.4151e-01$	$6.4270e-01$	–
Present Method for Example 5.3				
$\tilde{E}^{N,M}_{\varepsilon,\mu}$	$1.1380e-02$	$5.7551e-03$	$2.8963e-03$	$1.4538e-03$
$\mathfrak{R}^{N,M}_{\varepsilon,\mu}$	$9.8359e-01$	$9.9063e-01$	$9.9438e-01$	–
Result in [2](Upwind scheme on piecewise uniform mesh)				
$\tilde{E}^{N,M}_{\varepsilon,\mu}$	$1.3387e-02$	$1.1631e-02$	$8.6796e-03$	$5.8905e-03$
$\mathfrak{R}^{N,M}_{\varepsilon,\mu}$	$2.0280e-01$	$4.2236e-01$	$5.5922e-01$	–
Present Method for Example 5.4				
$\tilde{E}^{N,M}_{\varepsilon,\mu}$	$9.8180e-03$	$4.9629e-03$	$2.4969e-03$	$1.2535e-03$
$\mathfrak{R}^{N,M}_{\varepsilon,\mu}$	$9.8425e-01$	$9.9105e-01$	$9.9418e-01$	–
Result in [2](Upwind scheme on piecewise uniform mesh)				
$\tilde{E}^{N,M}_{\varepsilon,\mu}$	$2.1843e-02$	$1.7869e-02$	$1.2829e-02$	$7.8367e-03$
$\mathfrak{R}^{N,M}_{\varepsilon,\mu}$	$2.8973e-01$	$4.7804e-01$	$7.1108e-01$	–

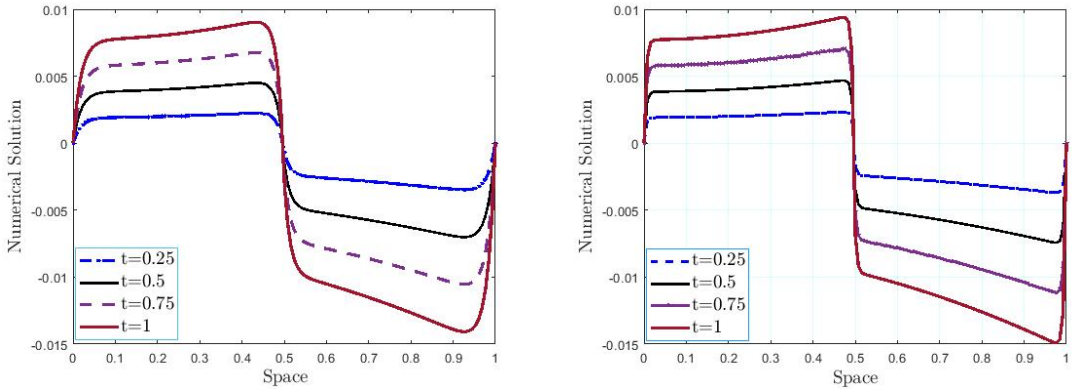

(a) $\varepsilon = 2^{-4}, \mu = 1$. (b) $\varepsilon = 2^{-8}, \mu = 2^{-12}$.

FIGURE 7. Line plots for Example 5.1.

Based on the research conducted by O'Riordan and Shishkin [19], it was found that the solution may contain an interior layer solely when the discontinuity is present in the convection-coefficient ($\varpi(x,t)$) is continuous). This numerical insight is crucial in understanding the behavior of solutions in the presence of discontinuities. It is evident

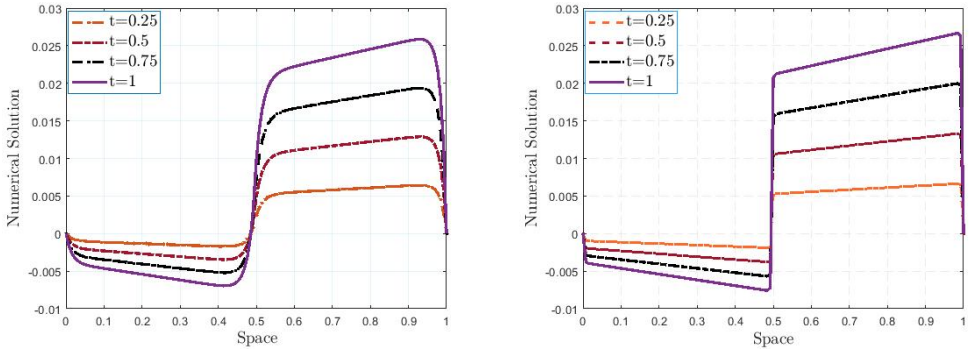

(a) $\varepsilon = 2^{-4}, \mu = 2^{-2}$. (b) $\varepsilon = 2^{-12}, \mu = 2^{-18}$.

FIGURE 8. Line plots for Example 5.2 at different time-levels.

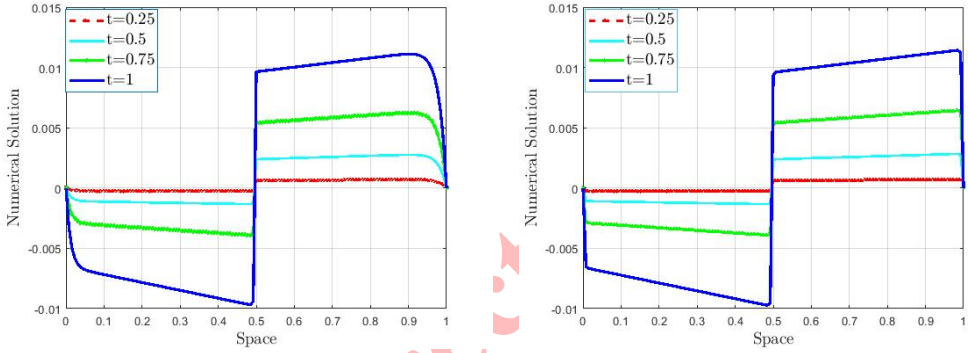

(a) $\varepsilon = 2^{-8}, \mu = 1$. (b) $\varepsilon = 2^{-12}, \mu = 2^{-8}$.

FIGURE 9. Line plots for Example 5.3 at different time-levels.

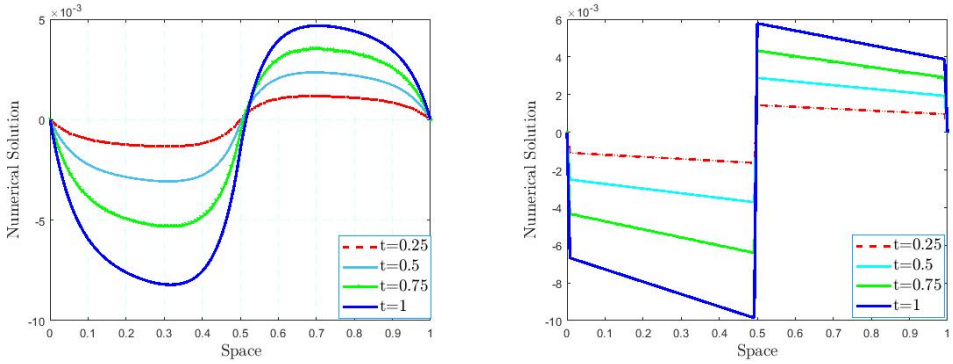

(a) $\varepsilon = 1, \mu = 2^{-6}$. (b) $\varepsilon = 2^{-16}, \mu = 2^{-16}$.

FIGURE 10. Line plots for Example 5.4 at different time-levels.

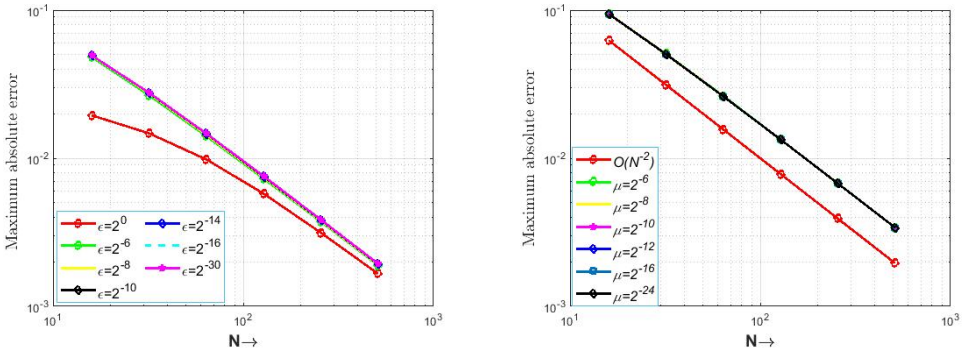

(a) Loglog plot for Example 5.1. (b) Loglog plot for Example 5.2.

FIGURE 11. The Loglog plot of maximum absolute error.

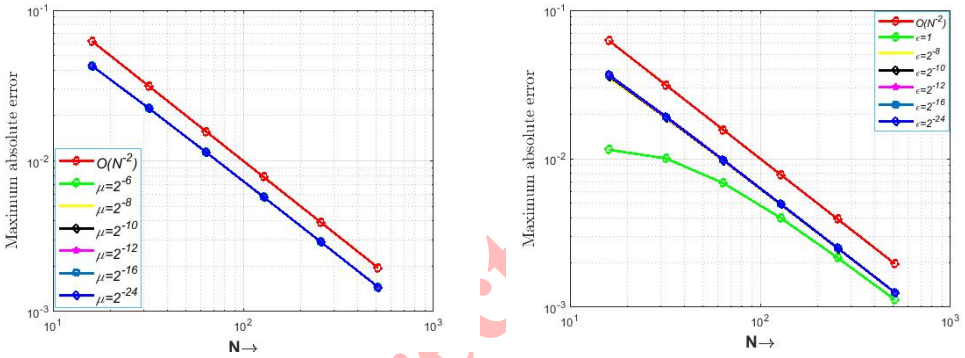

(a) Loglog plot for Example 5.3. (b) Loglog plot for Example 5.4.

FIGURE 12. The Loglog plot of maximum absolute error.

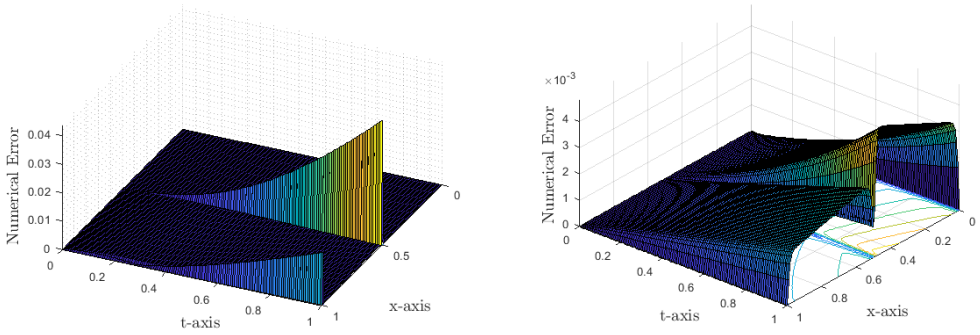

(a) $N = M = 128, \varepsilon = 2^{-18}, \mu = 2^{-8}$. (b) $N = M = 128, \varepsilon = 2^{-68}, \mu = 2^{-18}$.

FIGURE 13. Numerical error corresponding to Examples 5.2 and 5.4, respectively.

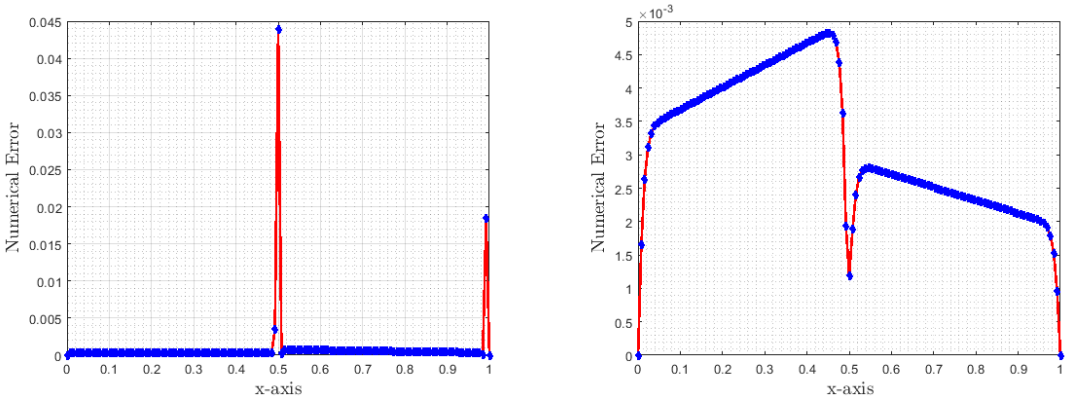

(a) $N = M = 128, \varepsilon = 2^{-18}, \mu = 2^{-8}$. (b) $N = M = 128, \varepsilon = 2^{-68}, \mu = 2^{-18}$.

FIGURE 14. Numerical error for Examples 5.2 and 5.4, respectively.

from Figure 6 that the solution might only contain the boundary layers if the discontinuity is in the convection-coefficient alone ($\varpi(x,t)$ is smooth). The discontinuous source functions in Example 5.4 are replaced with smooth function $\varpi(x,t) = (e^t - 1)(1+x)$ and $\varpi(x,t) = t(x-2)$, respectively, to draw Figures 6(a) and 6(b). For the modified examples, the solution surface plot at Figure 6 observes only the right and left boundary layers. In this context, the discontinuity in convection coefficient may only cause a shift in the layer within the solution. Despite the discontinuities in the convection coefficients, the interior layer phenomena might not manifest if the source functions are considered smooth. Surface plots of the error provide a clear depiction of the solution's behavior across the spatial and temporal domains, particularly in regions where sharp gradients or boundary layers occur. Figures 13(a) and 13(b) show the surface error plots for Examples 5.2 and 5.4, illustrating that the highest errors occur near the boundary and interior regions, as indicated by the prominent spikes. Similarly, Figures 14(a) and 14(b) present the line error plots for the same examples, confirming that the maximum errors are concentrated in these regions. Furthermore, to illustrate the practical validity of the expected rate of convergence, we have presented the error plots on a log-log scale in Figures 11 and 12, corresponding to Examples 5.1-5.4, respectively.

6. Conclusion

A computational approach is formulated to address a class of parabolic TP-SPPs characterized by jump discontinuities in the source and convection terms. The solution to this problem displays a unique layer behavior, influenced by the discontinuities and the presence of two small perturbation parameters. We propose a numerical scheme on a uniform mesh, using implicit Euler for time discretization and non-polynomial cubic splines for spatial direction. Rigorous testing and convergence analysis confirm its robustness, achieving first-order accuracy in time and second-order accuracy in space. Surface plots of four test problems reveal parabolic boundary layers along the lateral surfaces and interior layers near the discontinuity for small perturbation parameters. The proposed scheme's performance, both theoretically and numerically, matches the accuracy of existing difference schemes. Future research could extend this framework to higher dimensions, addressing challenges like managing boundary and initial layers and developing efficient schemes that ensure uniform convergence. Additionally, exploring adaptive mesh refinement to optimize grid resolution in critical regions will enhance both efficiency and accuracy.

Acknowledgment

The authors extend their gratitude to the anonymous referees for their meticulous review of the manuscript and for their valuable suggestions. This research did not receive any specific funding.

References

[1] P. H. Bhathawala and A. P. Verma, *A two-parameter singular perturbation solution of one dimension flow through unsaturated porous media*, Appl. Math., *43* (1975), 380–384.

[2] M. Chandru, P. Das, and H. Ramos, *Numerical treatment of two-parameter singularly perturbed parabolic convection diffusion problems with non-smooth data*, Math. Meth. Appl. Sci., *41* (2018), 5359–5387.

[3] M. Chandru, T. Prabha, and V. Shanthi, *A numerical method for solving interior layers parabolic problems with discontinuous convection-coefficient and source terms*, Diff. Equn. Dyn. Sys., *27* (2019), 91–112.

[4] M. Chandru, T. Prabha, and V. Shanthi, *A parameter robust higher order numerical method for singularly perturbed two parameter problems with non-smooth data*, J. Comput. Appl. Math., *309* (2017), 11–27.

[5] J. Chen and R. E. O'Malley, *On the asymptotic solution of a two-parameter BVP of chemical reactor theory*, SIAM J. Appl. Math., *26* (1974), 717–729.

[6] C. Clavero, J. L. Gracia, and G. I. Shishkin, *An efficient numerical scheme for 1D parabolic singularly perturbed problems with boundary layers*, J. Comput. Appl. Math., *318* (2017), 634–645.

[7] P. Das and V. Mehrmann, *Numerical solution of singularly perturbed convection-diffusion-reaction problems with two small parameters*, BIT Numer. Math., *56* (2016), 51–76.

[8] G. F. Duressa and T. B. Mekonnen, *An Exponentially Fitted Method for singularly Perturbed Parabolic BVP*, Commun. Korean Math. Soc., *38* (2023), 299–318.

[9] I. T. Daba and G. F. Duressa, *Computational method for singularly perturbed parabolic equations with discontinuous and large delay*, Heliyon, *8*(9) (2022).

[10] P. A. Farrell, A. F. Hegarty, J. J. H. Miller, E. O'Riordan, and G. I. Shishkin, *Global maximum norm parameter-uniform numerical method for a singularly perturbed convection-diffusion problem with discontinuous convection coefficient*, Math. Comput. Modell, *40*(11) (2004), 1375–1392.

[11] A. Jha and M. K. Kadalbajoo, *A layer adapted method for singularly perturbed two-parameter parabolic problems*, Int. J. Comput. Math., *92* (2015), 1204–1221.

[12] M. K. Kadalbajoo and K. C. Patidar, *A survey of numerical techniques for solving singularly perturbed ODEs*, Appl. Math. Comput., *130*(2-3) (2002), 457–510.

[13] D. Kumar and P. Kumari, *Uniformly convergent scheme for two-parameter singularly perturbed problems with non-smooth data*, Numer. Methods Partial Differ. Equ., *37*(1) (2021), 796–817.

[14] T. Lin and H. G. Roos, *Analysis of a FDM for a singularly perturbed problem with two small parameters*, J. Math. Anal. Appl., *289*(2) (2004), 355–366.

[15] T. B. Mekonnen and G. F. Duressa, *Nonpolynomial Spline Method for Singularly Perturbed Time-Dependent Parabolic Problem with Two Small Parameters*, Math. Probl. Eng., *2023* (2023).

[16] R. E. O'Malley, *Introduction to Singular Perturbations*, Academic Press, New York, 1974.

[17] R. E. O'Malley, *Two-parameter singular perturbation problems*, Doctoral Dissertation, Stanford University, USA, 1965.

[18] R. E. O'Malley, *Two-parameter singular perturbation problems for second order equations*, J. Math. Mech., *16* (1967), 1143–1164.

[19] E. O'Riordan and G. I. Shishkin, *Singularly perturbed parabolic problems with non-smooth data*, J. Comput. Appl. Math., *166*(1) (2004), 233–245.

[20] P. Ch. Podila and D. Kumar, *A uniformly convergent quadratic B-spline method for singularly perturbed partial differential equations with two small parameters*, J. Math. Chem., *59* (2021), 186–215.

[21] S. Singh, R. Choudhary, and D. Kumar, *An efficient numerical technique for singularly perturbed problems having discontinuity in convection coefficient and source term*, Comput. Appl. Math., *42*(1) (2023), 62.

[22] S. L. Cheru, G. F. Duressa, and T. B. Mekonnen, *Gaussian quadrature method with exponential fitting factor for two-parameter singularly perturbed parabolic problem*, BMC Research Notes, *17*(1) (2024), 304.

[23] S. L. Cheru, G. F. Duressa, and T. B. Mekonnen, *Numerical integration method for two-parameter singularly perturbed time delay parabolic problem*, Front. Appl. Math. Stat., *10* (2024), 1414899.